Dalton Transactions

ROYAL SOCIETY OF CHEMISTRY

PAPER

View Article Online
View Journal

Cite this: DOI: 10.1039/d0dt00928h

Octahedral copper(II)-diimine complexes of triethylenetetramine: effect of stereochemical fluxionality and ligand hydrophobicity on Cu^{II}/Cu^{I} redox, DNA binding and cleavage, cytotoxicity and apoptosis-inducing ability†

Mitu Sharma, [a] Mani Ganeshpandian, [b] Munmi Majumder,[c] Ajaykamal Tamilarasan, [d] Mukesh Sharma, [a] Rupak Mukhopadhyay, [c] Nashreen S. Islam *[a] and Mallayan Palaniandavar *[d]

Octahedral copper(II) complexes of the type $[Cu(trien)(diimine)](ClO_4)_2$ (**1–4**), where trien is triethylenetetramine and diimine is 2,2′-bipyridine (**1**), 1,10-phenanthroline (**2**), 5,6-dimethyl-1,10-phenanthroline (**3**), and 3,4,7,8-tetramethyl-1,10-phenanthroline (**4**), have been isolated. Single crystal X-ray structures of **1** and **2** reveal that the coordination geometry around Cu(II) is tetragonally distorted octahedral. The stereochemical fluxionality of the complexes illustrates the observed trend in Cu^{II}/Cu^{I} redox potentials and DNA binding affinity (K_b: **1**, 0.030 ± 0.002 < **2**, 0.66 ± 0.01 < **3**, 1.63 ± 0.10 < **4**, 2.27± 0.20 × 10^5 M^{-1}), determined using absorption spectral titration. All complexes effect oxidative DNA cleavage more efficiently than hydrolytic DNA cleavage. The bpy complex **1** with stereochemical fluxionality lower than its phen analogue **2** shows a higher cytotoxicity against both A549 lung (IC_{50}, 3.3 μM) and MCF-7 human breast (IC_{50}, 3.9 μM) cancer cells, and induces the generation of the highest amount of ROS in A549 cells. Complex **3** with a higher stereochemical fluxionality and higher ligand hydrophobicity exhibits a higher DNA binding and cleavage ability and higher cytotoxicity (IC_{50}, 2.1 μM) towards MCF-7 cells. Complex **4** with a still higher stereochemical fluxionality displays the highest DNA binding and cleavage ability but a lower cytotoxicity towards both A549 and MCF-7 cell lines due to its tendency to form a five-coordinated complex with the uncoordinated amine group. Annexin V.Cy3 staining and immunoblot analysis demonstrate the mechanism of cell death caused by **1** and **2**. The finding of the up-regulation of the pro-apoptotic Bax protein and down-regulation of PARP protein in western blot analysis confirms the induction of apoptosis by these complexes.

Received 11th March 2020,
Accepted 15th May 2020

DOI: 10.1039/d0dt00928h

rsc.li/dalton

Introduction

Cancer, the uncontrolled proliferation of cells, has become the main cause of death for the last 40–50 years.[1] In light of this, very intense research is being performed to develop a proper drug to fight against cancerous cells. Cisplatin, the first metal-based drug, is the most extensively used chemotherapeutic drug for the treatment of different types of cancers which include testicular cancer, cervical cancer, breast cancer, ovarian cancer, bladder cancer, and throat cancer, and for the treatment of brain tumors and many more.[2] Drugs such as carboplatin and oxaliplatin, known as the second generation platinum drugs, are also widely used in cancer treatment.[3a] High toxicity and resistance phenomena of cisplatin or other platinum drugs motivated researchers to develop new drugs with improved properties. Many Cu(II), Ru(II), Co(III), Ni(II), Zn(II) and Fe(III) complexes have been investigated as alternatives.[3b–f] Among all the metal complexes, those of copper and ruthenium are drawing wider attention as they are less toxic than platinum complexes. The best alternatives are synthetic Cu(II) complexes as copper is one of the essential bio-elements, and is important for growth, development, and

[a]Department of Chemical Sciences, Tezpur University, Tezpur 784 028, India
[b]Department of Chemistry, SRM Institute of Science & Technology, Kattankulathur, Chennai 603 203, Tamil Nadu, India
[c]Department of Molecular Biology and Biotechnology, Tezpur University, Tezpur 784 028, India
[d]School of Chemistry, Bharathidasan University, Tiruchirappalli 620 024, Tamil Nadu, India. E-mail: palanim51@yahoo.com

†Electronic supplementary information (ESI) available. CCDC 1884418 and 1884428. For ESI and crystallographic data in CIF or other electronic format see DOI: 10.1039/D0DT00928H

wound healing processes.[4] Also, copper ion has high affinity for nucleobases and has redox properties in the range of biological redox systems.[5–8] Furthermore, it plays an imperative role in the catalytic activity of many necessary enzymes. The synthesis of copper complexes by using various drugs as ligands is of great interest as they show excellent activity far better than that of free drugs.[9a] The antibacterial drugs coordinated to copper show a synergistic effect, which leads to various pharmacological activities such as antiproliferative, antiviral, and antifungal activity.[9] We have very recently studied the DNA cleaving property of complexes to investigate the role of nalidixic acid in cytotoxicity.[10] We have illustrated the DNA binding ability of many mixed ligand copper(II)-diimine complexes containing different primary ligands.[11,12] Iron and copper complexes can oxidatively cleave DNA by involving themselves in nucleobase oxidation and degrading sugar moieties through the abstraction of hydrogen atom(s) of deoxyribose. On the other hand, the complexes of copper(II) and zinc(II), which can act as strong Lewis acids, are suitable for the hydrolytic cleavage of DNA.[13]

Sigman and his coworkers reported the nuclease activity of a Cu(II) complex containing the 1,10-phenanthroline (phen) ligand, which can cleave double-stranded DNA in the presence of a reducing agent and molecular oxygen.[14,15] Sadler and his coworkers observed the cytotoxicity and antiviral activity of a mixed ligand bis(salicylato)Cu(II) complex with diimine co-ligands.[16] Burstyn and coworkers found that a copper(II) complex with macrocyclic triamine is involved in the hydrolytic cleavage of plasmid DNA.[17] We have isolated Cu(II) complexes of the type $[Cu(diimine)_3](ClO_4)_2$, where diimine is phen, 5,6-dimethyl-1,10-phenanthroline (5,6-dmp) and dipyrido[3,2-*d*:2′,3′-*f*]quinoxaline (dpq), and studied their ability to bind and cleave DNA.[18] In recent years, a large number of mixed ligand Cu(II) complexes have been found to exhibit antitumor activity by involving themselves in DNA adduct formation, DNA fragmentation and induction of apoptosis (programmed cell death).[10,14–25] We have correlated the DNA binding ability of many mixed ligand copper(II) complexes containing different primary ligands such as iminodiacetic acid,[20] L-tyrosine,[21] and 2-[(2-dimethylaminoethyl-imino)methyl] phenol.[22] Very recently, we have isolated a series of water-soluble mixed ligand Cu(II) complexes containing nalidixic acid as the primary ligand and phen, bpy, 5,6-dmp and 3,4,7,8-tetramethyl-1,10-phenanthroline (3,4,7,8-tmp) as co-ligands, and studied their interaction with CT DNA and their cytotoxicity.[10] Also, we have investigated a few families of mixed ligand Cu(II) complexes of the type $[Cu(3N)(diimine)]^{2+}$, where 3N is a linear tridentate ligand like dipicolylamine (dipica),[23] *N*,*N*-bis(benzimidzol-2-yl-methyl)amine (bba),[24] and *N*,*N*,*N*′,*N*″,*N*″-pentamethyldiethylenetriamine (pmdt), and correlated their DNA binding and cleavage ability with their cytotoxicity.[25]

Encouraged by the above results, we have now incorporated one more amine nitrogen donor to dien in $[Cu(dien)(diimine)]^{2+}$ to obtain mixed ligand octahedral Cu(II) complexes of the type $[Cu(trien)(diimine)](ClO_4)_2$ **1–4**, where trien is triethylenetetramine and diimine is bpy (**1**) or phen (**2**) or 5,6-dmp (**3**) or 3,4,7,8-tmp (**4**), as co-ligands (Scheme 1), with decreased lability. We wish to study the effect of incorporating the additional donor on the Cu(II) coordination geometry and DNA binding and cleavage ability and correlate them with cytotoxicity. It is to be noted that the dien ligand has been of interest for many years and the antimicrobial and dismutase activities of mixed ligand $[Cu(dien)(diimine)]^{2+}$ complexes have been studied.[9a] Now, trien has been chosen as the primary ligand as it has vast clinical applications, and exhibits apoptotic activity in murine fibrosarcoma cells. It can be used for cancer treatment as it exhibits telomerase inhibiting and anti-angiogenesis properties, and can overcome cisplatin resistance in the human ovarian cell line.[26] However, the study of trien as an anticancer agent is still scarce. Also, it is an important Cu(II) chelating agent that is used to bind and remove copper in the body in the treatment of Wilson's disease.[27a] Studies on Cu(II)-trien complexes have been performed vastly in order to treat diabetes mellitus and Alzheimer's disease also.[27b] A few metal-based trien complexes such as *cis*-$[Co(trien)(C_{11}H_{23}NH_2)Cl](ClO_4)_2$,[27c] *cis*-$[Co(trien)(C_{14}H_{29}NH_2)Cl]^{2+}$,[27d] and $[Cr^{III}(trien)(salicylate)]^{+}$,[27e] have been isolated and their DNA binding and cytotoxicity studies performed. Since the trien ligand as a free drug has many therapeutical applications, it can be made more permeable through the cell membrane by masking its hydrophilic group by binding to copper.[9a] In our laboratory, we have established that diimine co-ligands in the Cu(II) complexes of many primary ligands assist in DNA recognition and play an important role in the mechanism underlying chemical nuclease activity, and that the hydrophobic methyl substituents in the 5,6-dmp and 3,4,7,8-tmp co-ligands function as an hydrophobic DNA recognition element.[10] The complex $[Cu(trien)(5,6\text{-dmp})]^{2+}$ **3** displays a higher DNA binding affinity and higher cytotoxicity (IC_{50}, 2.21 μM) against MCF-7 breast cancer cell lines, while $[Cu(trien)(3,4,7,8\text{-tmp})]^{2+}$ **4** displays in general a higher DNA binding and cleavage but lower cytotoxicity towards both A549 and MCF-7 cancer cell lines.

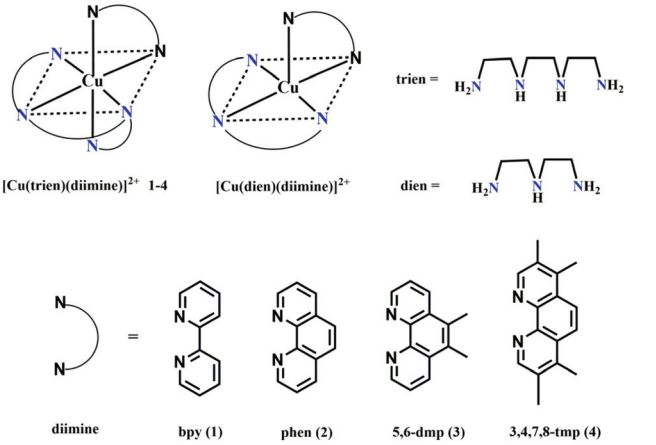

Scheme 1 Schematic representation of copper(II) complexes **1–4** and the diimine co-ligands.

Interestingly, the corresponding bpy complex (**1**), which shows a lower stereochemical fluxionality and higher Cu(II)/Cu(I) redox potential, exhibits the potential to kill many cancer cell lines with cytotoxicity (IC_{50}, 3.31 μM, A549) higher than its phen analogue. Both bpy (**1**) and phen (**2**) complexes induce apoptotic cell death, and the bpy complex is suggested as a potential compound to be further studied as a cytotoxic drug.

Experimental section

Materials

Copper(II) perchlorate hexahydrate (Alfa Aesar), triethylenetetramine (TCI chemicals, India), diethylenetriamine (Alfa Aesar), 2,2′-bipyridine, 1,10-phenanthroline, 5,6-dimethyl-1,10-phenanthroline (Aldrich), 3,4,7,8-tetramethyl-1,10-phenanthroline (3,4,7,8-tmp) and Calf Thymus (CT) DNA (highly polymerized and stored at 4 °C), ethidium bromide (EthBr), superoxide dismutase (SOD), catalase (Sigma, stored at −20 °C), pUC19 supercoiled plasmid DNA and agarose (Genei, Bangalore, India) were used as received. The cell lines MCF-7 and A549 were procured from the NCCS Pune, India. Cell culture media and reagents were purchased from Hi Media, India. 3-(4,5-Dimethylthiazolyl-2)-2,5-diphenyltetrazolium bromide (MTT) and Annexin V-Cy3.18 and Apoptosis Detection Kit were purchased from Sigma Aldrich, USA. All antibodies used in this study were procured from Cell Signaling Technology, USA. Ultra-pure Milli-Q water (18.2 μΩ) was used for all experiments. Commercial solvents were distilled and then used for the preparation of complexes. The complexes [Cu(dien)(bpy)]$(ClO_4)_2$ and [Cu(dien)(phen)]$(ClO_4)_2$ were prepared by following the procedure (ESI†) previously reported by Patel *et al.*[9a]

Synthesis of copper(II) complexes

Synthesis of [Cu(trien)(bpy)]$(ClO_4)_2$ (1). A methanolic solution of copper(II) perchlorate hexahydrate (0.40 g, 0.5 mmol) was added dropwise with stirring to a methanolic solution of triethylenetetramine (0.40 g, 0.5 mmol), and the stirring continued for 1 h at room temperature. A clear dark blue solution was obtained upon addition of a methanolic solution of 2,2′-bipyridine (0.078 g, 0.5 mmol) to the reaction mixture. The resulting solution was then stirred for 2 h at 40 °C, and a dark blue precipitate obtained was collected by filtration. Dark blue crystals, suitable for X-ray diffraction, were obtained by slow evaporation of the filtrate. Anal. calc. for [Cu(trien)(bpy)]$(ClO_4)_2$: C, 34.02; H, 4.64; N, 14.88; Cu, 11.25; found: C, 33.88; H, 4.50; N, 14.55; Cu, 10.89. λ_{max}/nm, in CH_3CN (ε_{max}/M^{-1} cm^{-1}): 574(160), 277(46 400), 242(37 000), 237(38 000). HR-MS (CH_3CN) displays a peak at *m*/*z* 522.1667 $[M - ClO_4 + CH_3CN + H_2O]^+$.

Synthesis of [Cu(trien)(phen)]$(ClO_4)_2$ (2). Complex **2** was prepared by adopting the procedure used for the synthesis of **1** but by using 1,10-phenanthroline (0.099 g, 0.5 mmol) instead of 2,2′-bipyridine. Upon crystallization, a dark blue crystalline solid was obtained, which was filtered off and then dried. It was found suitable for X-ray diffraction. Anal. calc. for [Cu(trien)(phen)]$(ClO_4)_2$: C, 36.71; H, 4.45; N, 14.27; Cu, 10.79; found: C, 36.47; H, 4.39; N, 14.11; Cu, 9.82. λ_{max}/nm, in CH_3CN (ε_{max}/M^{-1} cm^{-1}): 582(210), 265(41 330), 227(32 200), 202(24 400). HR-MS (CH_3CN) displays a peak at *m*/*z* 507.9254 $[M - ClO_4 + H_2O]^+$.

Synthesis of [Cu(trien)(5,6-dmp)]$(ClO_4)_2$ (3). Complex **3** was isolated by adopting the procedure used for the synthesis of **1** by using 5,6-dimethyl-1,10-phenanthroline (0.10 g, 0.5 mmol) in the place of 2,2′-bipyridine. Anal. calc. for [Cu(trien)(dmp)]$(ClO_4)_2$: C, 38.94; H, 4.90; N, 13.62; Cu, 10.30; found: C, 39.08; H, 4.73; N, 13.63; Cu, 9.89. λ_{max}/nm, in CH_3CN (ε_{max}/M^{-1} cm^{-1}): 591(153), 269(35 730), 233(44 800), 203(17 730). HR-MS (CH_3CN) displays a peak at *m*/*z* 551.2848 $[M - ClO_4 + 2H_2O]^+$.

Synthesis of [Cu(trien)(3,4,7,8-tmp)]$(ClO_4)_2$ (4). Complex **4** was isolated by adopting the procedure used for the synthesis of **1** by using 3,4,7,8-tetramethyl-1,10-phenanthroline (0.118 g, 0.5 mmol) instead of 2,2′-bipyridine. Anal. calc. for [Cu(trien)(3,4,7,8-tmp)]$(ClO_4)_2$: C, 40.97; H, 5.31; N, 13.03; Cu, 9.85; found: C, 41.06; H, 5.17; N, 12.88; Cu, 9.73. λ_{max}/nm, in (CH_3CN) (ε_{max}/M^{-1} cm^{-1}): 648(31), 275(46 330), 239(36 070), 211(45 600). HR-MS (CH_3CN) displays a peak at *m*/*z* 580.2500 $[M - ClO_4 + 2H_2O]^+$.

Experimental methods

Microanalyses (C, H and N) and atomic absorption spectroscopy (Cu) were carried out using a PR 2400 Series II PerkinElmer equipment and Thermo iCE 3000 series atomic absorption spectrophotometer (model analyst 200), respectively. A thermoscientific Exactive plus EMR mass spectrometer was employed for HR-MS analysis. The UV-Vis spectra were recorded on an Agilent Cary100 UV-Vis spectrophotometer using cuvettes of 1 cm path length. Electron Paramagnetic Resonance (EPR) spectra for the copper(II) complexes were obtained for polycrystalline compounds as well as in solution at LNT using a JEOL, Model: JES-FA200. Solutions of calf thymus (CT) DNA were prepared in buffer 5 mM Tris-HCl/50 mM NaCl buffer (pH, 7.2) in water giving a ratio of UV absorbance at 260 and 280 nm, A_{260}/A_{280}, of 1.9,[28,29] indicating that the DNA was sufficiently free of protein. Concentrated DNA stock solutions (14.8 mM) were prepared in a buffer and then sonicated for 25 cycles, with each cycle consisting of 30 s with an interval of 1 min.[10] The DNA concentration in nucleotide phosphate (NP) was obtained by absorbance at 260 nm after 1 : 100 dilutions by taking the extinction coefficient ε_{260} as 6600 M^{-1} cm^{-1}. The DNA stock solutions were stored at 4 °C and used before 5 days. Supercoiled plasmid pUC19 DNA was stored at −20 °C and the DNA concentration in base pairs was found by UV absorbance at 260 nm after suitable dilutions taking ε_{260} as 13 100 M^{-1} cm^{-1}. Concentrated stock solutions for all complexes were prepared in a CH_3CN solvent prior to the UV-Vis spectral analysis. Required amounts of these solutions were diluted with Tris buffer (5 mM Tris-HCl/50 mM NaCl buffer (pH, 7.2)) for measuring the UV-Vis absorption spectra. Cyclic voltammetry (CV) was performed on a platinum sphere electrode. Voltammetry studies were performed using a CHI-600E series CH Instrument. A three-electrode system con-

sisting of a platinum wire, a glassy carbon working electrode and an Ag/AgCl reference electrode were used. The supporting electrolyte was 0.1 M TBAB (tetra-butylammonium bromide) in Milli-Q water. The CV responses were obtained at ambient temperatures under N_2.

X-ray crystallography

The molecular structures of compounds **1** and **2** were determined unambiguously by measuring X-ray intensity data on a Bruker SMART APEX II single crystal X-ray CCD diffractometer at ambient temperature having graphite-monochromatized Mo-Kα (λ = 0.71073 Å) radiation. The data were resolved using direct procedures with SHELXS and refined by SHELXL-2013.[30] PLATON was used as the graphics interface package, and the figures were generated using the ORTEP 3.07 generation package.[31] The locations on all the atoms were obtained by straight methods. E-maps were used for the positioning of metal atoms in each complex, and non-hydrogen atoms were refined anisotropically. The hydrogen atoms bound to the carbon were first placed in geometrically controlled positions and then refined with isotropic temperature factors, generally 1.2 U_{eq} of their parent atoms. The crystallographic data are listed in Table 1.

Computational studies

The geometry optimization of all Cu(II) mixed ligand complexes were performed in CH_3CN solvent by using density functional theory (DFT) methods. LANL2DZ basis sets were used for describing the Cu metal atom with the Becke3–Lee–Yang–Parr hybrid functional (B3LYP), and for non-metal atoms, the 6-31G* basis sets were used. All DFT calculations were carried out by using the Gaussian 09 program package.[32a,b] Normal mode analyses were carried out to check the minimal energy nature of the geometry. The metal was considered in the +2 oxidation state and doublet spin state.

Table 1 Crystal data and structure refinement details for [Cu(trien)(bpy)]$(ClO_4)_2$ **1** and [Cu(trien)(phen)]$(ClO_4)_2$ **2**

	1	**2**
Sum formula	$C_{16}H_{26}Cl_2Cu\ N_6O_8$	$C_{18}H_{26}Cl_2CuN_6O_8$
Formula weight	564.87	588.89
Temperature (K)	100(2)	100(2)
Wavelength (Å)	0.7107	0.7107
Crystal system	Monoclinic	Monoclinic
Space group	$P2_1/c$	$P2_1/c$
a (Å)	11.562(3)	11.822(2)
b (Å)	14.067(4)	13.985(3)
c (Å)	13.652(4)	13.983(3)
α (°)	90	90
β (°)	91.830(4)	93.685(2)
γ (°)	90	90
Volume (Å^3)	2219.3(11)	2307.0(8)
Z	4	4
D_c (g cm^{-3})	1.691	1.695
Reflections collected	3897	6184
Goodness-of-fit on F^2	1.107	0.913
Final R indices [$I > 2\sigma(I)$]	0.0595, wR_2 = 0.1806	0.0469, wR_2 = 0.1060
R indices (all data)	0.0654, wR_2 = 0.1902	0.0666, wR_2 = 0.1172

For DNA docking study, the optimization of the coordination geometries of the mixed ligand Cu(II) complexes was performed using Avogadro, a molecular editor and visualizer tool, and the DNA molecule (PDB ID: 1BNA) was considered in this study. The initial coordinates were taken from the single-crystal X-ray data of **1** and **2**. The DNA docking with complexes was done using the PatchDock server, which is a molecular docking algorithm based on complementarity principles. PatchDock usually finds the optimum candidate solutions from the list of all possible solutions, using RMSD (Root Mean Square Deviation) clustering to eliminate redundant solutions, which is based on the geometry docking algorithm.[33a,b] It forms a set of two molecules by computing the three-dimensional transformations of one of the molecules with respect to the other in order to maximize surface shape complementarity and minimize the number of steric clashes. On the basis of geometric fit as well as atomic desolvation energy,[34] a particular score was assigned to each solution. In this study, we chose 4 Å as the default RMSD value and used it for clustering solutions. The conformer having the negative atomic contact energy (ACE) value, highest interface area, and complementary geometric score was obtained from the PatchDock online server. The Fire Dock server was employed to analyze the refinements of the structures obtained from PatchDock, and is based on the Global energy algorithm, which gives a description of the refinement problem of complex docked solutions.[35] This server refines and scores the candidate models, conferring an energy function. Side-chain conformations and rigid-body orientation were used to optimize the solution of the candidate. Rotamers model the side-chain flexibility, and the obtained combinatorial optimization problems are resolved by integer linear programming.[36] It mainly targets the flexibility problem and solution scoring formed by fast rigid-body docking algorithms. According to an energy function, FireDock spends about 3.5 seconds per candidate solution to refine a set of 1000 potential docking candidates.[35]

DNA binding and DNA cleavage experiments

The DNA binding (ESI†) and DNA cleavage studies were carried out by employing the procedure reported by us previously.[10]

Cell culture

The MCF-7 and A549 cell lines were routinely maintained in Dulbecco's modified Eagle's medium (DMEM) supplemented with 10% FBS and 1% antibiotic. The cell lines were kept in a CO_2 incubator at 5% CO_2 and 37 °C temperature.

Cytotoxicity assay

The 3-(4,5-dimethylthiazol-2-yl)-2,5-diphenyl tetrazolium bromide (MTT) colorimetric assay was carried out as described by Mosmann.[37] Cells were trypsinized from confluent flasks and counted using a haemocytometer. In each well of a 96 well plate, 5000 cells were plated and incubated for 24 h. All complexes were first dissolved in a small volume of DMSO and the solution diluted with cell culture media. All treatments were

done at non-toxic concentrations of DMSO, *i.e.* less than 0.02%. Also, prior to assessing the anti-proliferative activity, the time-dependent stability of the complexes was checked in the buffer medium used for the MTT assay up to 72 h. No significant changes were observed in the UV-Vis absorption spectral bands of complexes upon standing, indicating that the complexes would maintain their identity while performing the cellular experiments. The cells were treated with different concentrations of the complexes followed by incubation for 48 h. They were then treated with 20 μL of MTT solution (5 mg mL^{-1}) and incubated for 3.5 h. The media were removed carefully and a 150 μL MTT dissolving solution (11% SDS in a 1 : 1 ratio of 0.2 M HCl : isopropanol) was added.[37,38a] The absorbance of the solutions was measured at 580 nm using a UV-Vis spectrophotometer (Multiscan Go, Thermo Scientific, USA). The effective concentration of the complexes was found in the range that was used in the MTT assay, that is, 2.5 to 50 μM. The IC_{50} values of the complexes were obtained by extrapolating the best fit cytotoxicity curve obtained by using the online software Graph Pad prism.[38b] The data were calculated for three replicates each and used to calculate the mean.

Intracellular ROS determination

In a 96 well plate 25 000 cells per well were seeded in 100 μL complete DMEM media overnight. The cells were washed with PBS and incubated with 50 μL of 2′,7′-dichlorofluorescin diacetate (DCFDA) at a concentration of 40 μM in each well with cells for 45 min. After that each well containing the cells was washed with PBS and the cells were treated with different contraptions of the four complexes (**1–4**) in PBS for 6 h. The cells were then lysed by lysis buffer in each well without washing them and fluorescence was measured at an excitation and emission wavelength of 504 and 529 nm respectively, and fluorescence intensity was calculated with respect to control. 1 mM H_2O_2 was used as a positive control in the experiment.

DNA fragmentation assay

MCF-7 and A549 cells were plated in 35 mm dishes, counting 0.5×10^6 cells per dish and incubated for 24 h. The cells were then treated with complex **1** (4, 8 μM) and **2** (10, 20 μM) for 0, 24, and 48 h. The treated cells were trypsinized and genomic DNA was isolated using the PureLinkTM Genomic DNA Mini Kit (Invitrogen, USA) following the manufacturer's protocol. Concentrations of the isolated genomic DNA were measured and run on a 2% agarose gel.

Annexin V.Cy3 assay

The MCF-7 and A549 cells were plated in 96 well plates (10 000 cells per well) and allowed to seed overnight. The cells were treated with complex **1** (4, 8 μM) and **2** (10, 20 μM) for 24 h. The media were removed carefully and Annexin V-Cy3.18 conjugate and 6-carboxyfluoresceindiacetate (6-CFDA) were added according to the manufacturer's protocol.[39] After incubation for 10 min, fluorescent images were taken from five different fields of each well using a fluorescence microscope Model Olympus IX83 (Japan), and the cells were counted manually.

Western blot analysis

The MCF-7 and A549 cells were seeded in a 60 mm dish at 1×10^6 cells per dish overnight and treated with either complex **1** or **2** for 24 h. Proteins were extracted from the treated and untreated cells using RIPA buffer. An equal amount of proteins from different experimental samples were run in a 10% resolving SDS-PAGE and the proteins were transferred to a 0.22μ PVDF membrane using a semi-dry electrophoresis transfer unit (GE Healthcare, UK). The membranes were blocked with 5% non-fat dry milk in TBS-Tween 20 (TBST) for at least 3 h at room temperature to prevent non-specific binding. The membranes were washed with TBST five times for 10 min each and probed with the corresponding primary antibodies (anti-Bax, anti-PARP, and anti-β-actin) at 1 : 1000 dilutions overnight at 4 °C. The membranes were again washed and incubated with secondary antibodies for 1 h at room temperature. The blots were then incubated with chemiluminescence substrate (Bio-Rad, USA) and visualized using a Chemidoc XRS + system (Bio-Rad, USA). Quantification of the bands was done using Gel Quant software.

Results and discussion

Characterization of copper(II) complexes

Four mixed ligand complexes of the type [Cu(trien)(diimine)]$(ClO_4)_2$ (**1–4**), where trien is triethylenetetramine and diimine is bpy (**1**) or phen (**2**) or 5,6-dmp (**3**) or 3,4,7,8-tmp (**4**), were isolated by using simple synthetic procedures and were characterized using different analytical and spectroscopic techniques. All complexes are insoluble in water but soluble in organic solvents like acetonitrile, methanol, *etc*. The formulae of the complexes were determined based on elemental analyses and HR-MS (Fig. S1a–d†), and the stoichiometry of complexes **1** and **2** was confirmed by determining their X-ray crystal structures (*cf.* below). In the IR spectra, a broad band in the range of 1080–1091 cm^{-1} and a strong and sharp band near 620 cm^{-1} are observed for all complexes, which are characteristic of uncoordinated ionic perchlorates.[40,41] The most significant medium intensity bands observed in the region 3080–3380 cm^{-1} are assigned to the ν(N–H) vibration, and the bands in the region 1422–1434 cm^{-1} are assigned to pyridine-based vibrations (Fig. S2†).[40,42] The HR-MS data in acetonitrile solution reveal that the complexes maintain their identity in solution, which is supported by their molar conductivity in methanol solution (Λ_M/Ω^{-1} cm^2 mol^{-1}: 237–260) falling in the range of 1 : 2 electrolytes.[43,44]

Structures of [Cu(trien)(bpy)]$(ClO_4)_2$ 1 and [Cu(trien)(phen)]$(ClO_4)_2$ 2

The ball and stick representations of [Cu(trien)(bpy)]$(ClO_4)_2$ **1** and [Cu(trien)(phen)]$(ClO_4)_2$ **2**, including the atom numbering scheme, are shown in Fig. 1(a) and (b), respectively, and the unit cell packing diagrams are shown in Fig. S3.† The crystal structure refinement data and selected bond lengths and bond angles are listed in Tables 1 and 2, respectively. The crystallo-

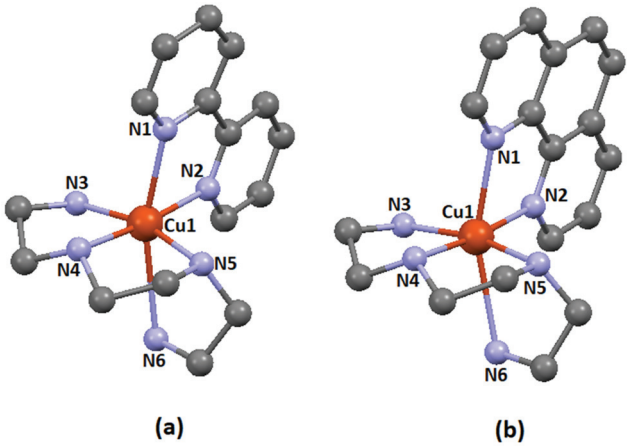

Fig. 1 Ball-and-stick representation of the crystal structures of [Cu(trien)(bpy)]$(ClO_4)_2$ **1** (a) and [Cu(trien)(phen)]$(ClO_4)_2$ **2** (b). Hydrogen and perchlorate atoms are omitted for clarity.

Table 2 Selected bond lengths (Å) bond angles (°) for [Cu(trien)(bpy)]$(ClO_4)_2$ **1** and [Cu(trien)(phen)]$(ClO_4)_2$ **2**

1		**2**	
Bond length		Bond length	
Cu1–N1	2.307(4)	Cu1–N1	2.326(2)
Cu1–N2	2.054(4)	Cu1–N2	2.032(3)
Cu1–N3	2.026(4)	Cu1–N3	2.028(2)
Cu1–N4	2.021(4)	Cu1–N4	2.013(3)
Cu1–N5	2.027(4)	Cu1–N5	2.042(2)
Cu1–N6	2.723(4)	Cu1–N6	2.670(3)
Bond angle		Bond angle	
N2–Cu1–N4	174.1(2)	N2–Cu1–N4	173.6(1)
N5–Cu1–N3	164.8(2)	N3–Cu1–N5	167.3(1)
N1–Cu1–N6	163.3(1)	N1–Cu1–N6	160.23(9)
N2–Cu1–N5	98.6(2)	N2–Cu1–N5	98.5(1)
N4–Cu1–N3	84.0(2)	N3–Cu1–N4	84.3(1)
N2–Cu1–N1	75.9(1)	N2–Cu1–N1	77.15(9)
N6–Cu1–N5	73.7(2)	N5–Cu1–N6	74.0(1)
N1–Cu1–N3	99.8(1)	N3–Cu1–N1	99.83(9)
N4–Cu1–N6	89.3(2)	N4–Cu1–N6	91.1(1)

graphic asymmetric unit cell of **1** contains one complex cation and two lattice perchlorate anions. Cu(II) in the complex is coordinated by six nitrogen atoms, all four nitrogen atoms of trien (N3, N4, N5, and N6) and both nitrogen atoms (N1 and N2) of bpy to form a distorted octahedral coordination geometry. The N2 nitrogen of bpy (Cu1–N2, 2.054 Å) and N3, N4, and N5 nitrogen atoms of trien constitute the square plane (Cu1–N3, 2.026; Cu1–N4, 2.021; Cu1–N5, 2.027 Å) of the octahedron, while the N1 nitrogen of bpy and the N6 nitrogen of trien occupy the axial positions at longer distances (Cu1–N1, 2.307; Cu1–N6, 2.723 Å), which is expected due to the presence of two electrons in the d_{z^2} orbital of Cu(II) (the Jahn–Teller effect). The octahedral complex is tetragonally distorted ($T = R_{in}/R_{out}$ = 0.804),[18,45–47] where R_{in} = (2.054 + 2.026 + 2.021 + 2.027 Å)/4 and R_{out} = (2.723 + 2.307 Å)/2, suggesting that the complex shows a 'static' Jahn–Teller distortion.[18] The trien ligand shows *cis*-β, rather than *cis*-α conformation, in which the 4N ligand adopts a partially folded arrangement. A 3D continuum of the trien ligand is formed by the face to face π–π intramolecular C–H–π interactions of the adjacent pyridyl plane.[42] The sum (Σ) of the bond angles (N2–Cu1–N4, 174.10(2)°; N3–Cu1–N5, 164.80(2)°) around Cu(II) is 338.90°, revealing that the equatorial plane around Cu(II) in **1** is not perfectly square planar, in agreement with a distorted octahedral coordination geometry.[48–50] Also, the cisoid and transoid angles are found to be in the range of 85.8–92.4 and 164.8–174.1°, respectively, similar to those found in the [Ni(trien)(bpy)]$(ClO_4)_2$ complex.[42] They deviate significantly from the ideal angles of 90° and 180°, confirming that the coordination geometry is distorted octahedral. The unit cell of [Cu(trien)(phen)]$(ClO_4)_2$ **2** also contains a complex cation and two lattice perchlorate anions. The complex shows a distorted octahedral coordination geometry similar to **1**. Thus, Cu(II) is located at the center of a distorted octahedral geometry with phen N2 (Cu1–N2, 2.032 Å), and trien N5 (Cu1–N5, 2.042 Å), N4 (Cu1–N4, 2.013 Å) and N3 (Cu1–N3, 2.028 Å) nitrogen atoms occupying the corners of the distorted square plane, while N1 of phen (Cu1–N1, 2.326 Å) and N6 of trien (Cu1–N6, 2.670 Å) in the axial positions at longer distances as in **1**. The slight deviation of the sum (Σ, 340.90°) of the bond angles (N2–Cu1–N4, 173.60(1)°; N3–Cu1–N5, 167.30(1)°) from the theoretical value of 360° around Cu(II) in **2** indicates that the square planar environment is quite distorted. Complex **2**, like **1**, possesses a predominantly *cis*-β rather than a *cis*-α configuration.[41,51] Also, it is tetragonally distorted ($T = R_{in}/R_{out}$ = 0.812) suggesting that the octahedral complex shows a 'static' Jahn–Teller distortion, but lower than its bpy analogue **1** (*T*, 0.804) and hence possesses a higher 'fluxional' stereochemistry.[18,42,52a] The lower value of *T* for **1** originates from the σ-bonding of non-planar bpy more strongly than phen (pK_a, $bpyH^+$, 4.4; $phenH^+$, 4.9)[52b] in the axial direction (**1**, 2.307; **2**, 2.326 Å), which weakens the Cu–N_{amine} bond *trans* to it more than that in **2** (Cu1–N6: **1**, 2.723; Cu1–N6: **2**, 2.670 Å). Also, the equatorial bond formed by bpy is weaker than that formed by phen (Cu1–N2: **1**, 2.054; **2**, 2.032 Å), which is expected due to the stronger π-back bonding of the more delocalized phen in the equatorial plane. Also, the equatorial Cu–$N_{diimine}$ bonds in **1** and **2** are weaker than the Cu–N_{amine} bonds of trien located *trans* to them. So, it is clear that both bpy and phen co-ligands would contribute to the overall electronic properties of the Cu(II) complexes with a Jahn–Teller distortion. Thus, the bpy complex with a higher static coordination geometry shows an LF strength higher than its phen analogue (*cf.* below). We have observed earlier that the tetragonality index of [Cu(phen)$_3$]$(ClO_4)_2$ is lower (*T*, 0.875) than that (*T*, 0.952) of [Cu(5,6-dmp)$_3$]$(ClO_4)_2$, on account of the incorporation of electron-releasing methyl substituents on phen ring *trans* to heterocyclic nitrogen donors on 5,6-dmp.[18] Similarly, it is expected that the 5,6-dmp (**3**) and 3,4,7,8-tmp (**4**) complexes would exhibit a stronger axial Cu–N bond and hence confer values of *T* higher than the phen analogue **2**, and confer a lower LF strength. It is unfortunate that suitable single crystals of these complexes could not be obtained to verify the predication. However, DFT calculations (*cf.* below)

reveal that the equatorial Cu–$N_{diimine}$ bond lengths for the octahedral complexes **3–4** are longer than that for **2**, leading to T values slightly higher than that for **2**.

It is interesting to compare the structures of **1** and **2** with those of the dien analogues[9a] [Cu(dien)(bpy)]$(BF_4)_2$ and [Cu(dien)(phen)]$(ClO_4)_2$ respectively, which show a trigonal bipyramidal distorted square planar (TPDSP) geometry (trigonality index τ: bpy, 0.14; phen, 0.11) with the dien ligand coordinated meridionally. When an amino nitrogen is incorporated in these dien complexes to give **1** and **2**, it occupies the vacant axial position at longer distances. Consequently, the *trans* axially located nitrogen atoms (N1) of bpy and phen are displaced to longer distances (**1**, 2.229 to 2.307 Å; **2**, 2.186 to 2.326 Å) and three of the four equatorial Cu–N bonds (**1**: 1.980 to 2.054; 1.987 to 2.026; 2.016 to 2.021; 2.054 to 2.027 Å; **2**: 2.022 to 2.032; 2.011 to 2.028; 2.005 to 2.013; 2.040 to 2.042 Å) are elongated.

Structures of copper(II) complexes: density functional theory calculations

Geometry optimization for **1–4** has been carried out using density functional theory (DFT). The initial coordinates for **1** were taken from the single-crystal X-ray data of [Cu(trien)(bpy)]$^{2+}$ **1** and the structure subjected to optimization. The optimized structures of **1–4** are shown in Fig. S4† and the geometrical parameters *viz.* bond lengths, optimized energies, frontier MOs, and SOMO–SOMO+1 energy gap have been calculated (Table 3, Fig. 2 and S5†) at the B3LYP 6-31G/LANL2DZ levels using the Gaussian 09 program package. The computed structural parameters for **1** and **2** agree well with those in their X-ray crystal structures; however, the computed Cu–N6 bond length of both of them is about 0.2 Å shorter and the computed Cu–N1 bond length is about 0.1 Å longer than those found in their X-ray structures, which is attributed to the overestimation of covalency of Cu(II) by the established exchange–correlation function, which is well-recognized.[32b] The tetragonality indexes for **1** (*T*, 0.830) and **2** (*T*, 0.830) calculated from the computed bond angles, though the same, are closer to the

Table 3 Computed structural parameters and values of the HOMO–LUMO energy gap in complexes **1–4**

Parameters	1	2	3	4
Bond Lengths [Å]				
Cu–N(1)	2.417	2.470	2.427	2.432
Cu–N(2)	2.090	2.093	2.086	2.081
Cu–N(3)	2.083	2.081	2.083	2.083
Cu–N(4)	2.069	2.065	2.068	2.066
Cu–N(5)	2.099	2.097	2.099	2.101
Cu–N(6)	2.555	2.512	2.553	2.555
Optimized energy (eV)	-3.13×10^4	-3.34×10^4	-3.55×10^4	-3.76×10^4
SOMO (HOMO) (eV)	−7.0437	−7.0537	−6.8992	−6.9609
SOMO+1 (LUMO) (eV)	−2.6493	−2.6411	−2.5843	−2.4069
HOMO–LUMO energy gap (eV)	−4.3944	−4.4126	−4.3149	−4.5541

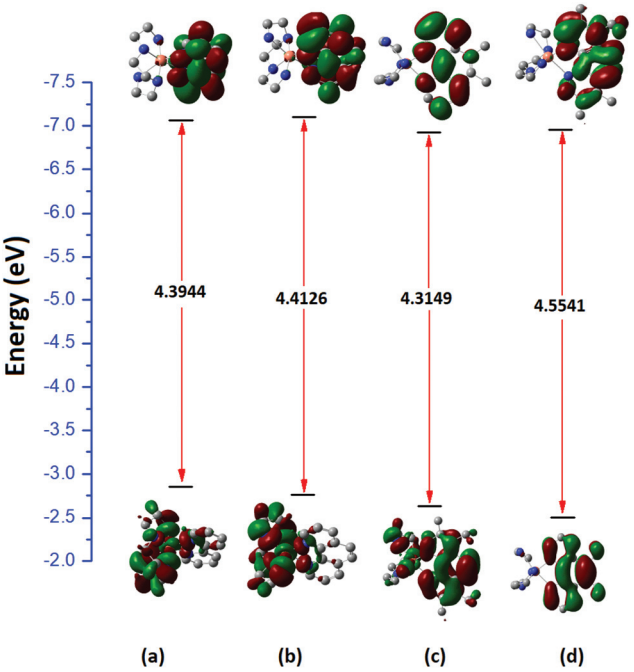

Fig. 2 Energy profile diagram of complexes [Cu(trien)(bpy)]$^{2+}$ **1** (a), [Cu(trien)(phen)]$^{2+}$ **2** (b), [Cu(trien)(5,6-dmp)]$^{2+}$ **3** (c) and [Cu(trien)(3,4,7,8-tmp)]$^{2+}$ **4** (d). The doublet spin state: HOMO and LUMO in restricted spin calculations were carried out at TD–DFT using the B3LYP dispersion corrected functional level with the 6-31G/LANL2DZ basis set as implemented in the Gaussian 09 package.

experimental values (*cf.* above). Apart from these, there are no significant differences in the bond length and spin densities of **1–4**. Thus, as the method of calculation adopted could reproduce the distorted octahedral structures of **1** and **2**, the computed structures of **3** and **4** are reliable and are suitable for structural discussions. The tetragonality indexes for **3** (0.836) and **4** (0.834) are slightly higher than those calculated for **1** and **2**. However, the incorporation of methyl groups, as in [Cu(5,6-dmp)$_3$]$^{2+}$, is expected to decrease the axial bond length and hence increase the value of the tetragonality index *T* significantly (*cf.* above).[18]

It is interesting that the singly occupied molecular orbital (SOMO/α spin) is localized entirely on the trien ligand in **1** and **2**, completely on the 5,6-dmp ligand in **3** and both on trien (less than in **1** and **2**) and 3,4,7,8-tmp (less than in **3**) in **4**, and the β spin density of SOMO is always localized on the trien ligand irrespective of the co-ligand. As frontier molecular orbital approximation indicates that SOMO determines the electron-releasing ability of the ligand, the highest value of the SOMO energy of **3** (**3** (−6.8992) > **4** (−6.9609) > **1** (−7.0437) > **2** (−7.0537 eV)) reveals that the 5,6-dmp ligand releases more electrons, as the methyl substituents are positioned *trans* to the heterocyclic nitrogen donors into the unoccupied orbital of the metal ion, and hence are involved in the strongest σ-bonding to Cu(II). Thus, the σ-donor capability of the primary ligand trien is tuned by the variation in the diimine co-ligand, which reflects the presence of synergy between the primary

and secondary ligands when bound to the metal. The energy of the SOMO+1 orbitals localized largely on the diimine co-ligand corresponds to the ability of the co-ligand to accept electrons, and the observed trend in the energy of SOMO+1, **1** (−2.6493) < **2** (−2.6411) < **3** (−2.5843) > **4** (−2.4069 eV) illustrates that the π* orbital of bpy and phen are delocalized more than those in 5,6-dmp (**3**) and 3,4,7,8-tmp (**4**) and that the π* orbital in **4** is less delocalized than that in **3**. Therefore, the more delocalized π* orbital of phen would be involved in a stronger π back-bonding with Cu(II) to stabilize the Cu(I) oxidation state more than what 5,6-dmp and 3,4,7,8-tmp co-ligands do. This is in good agreement with the observed trend in $E_{1/2}$ values illustrating that delocalization of the π* orbital of co-ligands is important in stabilizing the lower oxidation of Cu (I) (*cf.* below). The variation in the SOMO–SOMO+1 energy gap calculated, *viz*. **1** < **2** > **3** < **4**, reveals that the metal to ligand charge transfer (MLCT) band energy is expected to vary in this order.

Spectral and electrochemical properties of copper(II) complexes

In acetonitrile solution, all complexes show a ligand field (LF) band with very low absorptivity (λ_{max}, 574–648 nm; ε_{max}, 100–210 M^{-1} cm^{-1}), which is consistent with the tetragonally distorted octahedral geometry observed in the X-ray crystal structures of **1** and **2** and the optimized structures of all complexes (Table S1 and Fig. S6†).[18] The LF band energy varies in the order **1** > **2** > **3** > **4**, suggesting that the σ-bonding of non-planar bpy nitrogen atoms confers a stronger ligand field than the π back-bonding of the phen ring (*cf.* above). The incorporation of four methyl substituents as in **4** decreases the π back-bonding of the phen ring more than that of the two methyl substituents as in **3** and hence the LF energy of **4** is much lower (50 nm) than that of **3**. The complexes exhibit an intense absorption band in the UV region (200–280 nm; ε_{max}, 24 400–46 400 M^{-1} cm^{-1}), which is attributed to the intraligand π → π* and n → π* transitions in the aromatic chromophores of the complexes.[10] The UV-Vis spectral features of **1–3** in Tris-buffer solution do not differ much from those obtained in CH_3CN solution, confirming that the octahedral complexes maintain their identity even in buffer solution. The polycrystalline EPR spectra of the complexes are axial as expected, with the parallel component for **1** resolved ($g_{\|}$, 2.250; $g_{\perp}$, 2.070) while that for **2** ($g_{\perp}$, 2.090) and **3** ($g_{\perp}$, 2.094) not resolved. The polycrystalline EPR spectrum of **4** contains spectral features characteristic of the dimeric Cu(II), with the $\Delta S = \pm 2$ half-field signal appearing at 1650 G. The complex $[Cu(dien)(phen)]^{2+}$ has been shown to have two molecules of the same kind brought together by building a network of H-bonds, with the distance between two copper atoms being 0.29 Å.[9a] A similar molecular structure is suggested for **4** with the fourth amino nitrogen remaining uncoordinated, possibly due to the stronger σ-bonding of the 3,4,7,8-tmp co-ligand, but weakly co-ordinated axially to copper(II) of the neighboring complex molecule in the solid state; however, in solution, the dimeric copper(II) structure is unstable (no half-field signal is observed), and it dissociates to give monomeric copper(II) species like **1–3**. It is unfortunate that we could not obtain suitable single crystals of **4** to verify the dimeric structure. The frozen solution EPR spectra of **1–4** are axial with $g_{\|} > g_{\perp} > 2.0$ and $G = [(g_{\|} - 2)/(g_{\perp} - 2)] = 3.5–4.5$, which is in agreement with the square-based geometry found in the X-ray crystal structures of **1** and **2**. A square-based CuN_4 chromophore is expected to show a $g_{\|}$ value of around 2.200 and an $A_{\|}$ value in the range of 180–200 × 10^{-4} cm^{-1}. On the other hand, distortion from square planar coordination geometry would increase the $g_{\|}$ value and decrease the $A_{\|}$ value.[53,54,55a] The observed $g_{\|}$ and $A_{\|}$ values from the frozen solution spectrum ($g_{\|}$, 2.203–2.206; $A_{\|}$, 173–189 × 10^{-4} cm^{-1}) are consistent with the presence of a tetragonally distorted CuN_6 chromophore[45–47] with significant axial interaction, as in the X-ray crystal structure of **1** (Table S1 and Fig. S7–S9†).

The cyclic voltammetry (CV) responses obtained in acetonitrile solution reveal that the Cu(II)/Cu(I) redox couples ($E_{1/2}$, 0.123 to −0.139 V, Table S2 and Fig. S10†) of **2** and **3** are more reversible than those of **1** and **4**.[10] The $E_{1/2}$ values vary in the order **1** (0.123) > **2** (−0.085) > **3** (−0.129) > **4** (−0.139 V), which is consistent with the variation in the LF band energy (*cf.* above). The phen complex **2** is more easily reducible than **3** with the π* orbital of the phen ring substituted with two methyl groups being less delocalized than that of the phen ring, and similarly **4**, with the phen ring substituted with four methyl groups being much less delocalized, exhibits a still lower redox potential. The more π-delocalized phen ring in **2** is expected to stabilize Cu(I), while the less planar pyridyl rings in **1** (*cf.* above) are expected to stabilize Cu(II), conferring a more negative Cu(II)/Cu(I) redox potential on **1**. However, interestingly, the Cu(II)/Cu(I) redox potential of **1** is observed to be more positive than that of **2**. We have already established[18,55b] that among octahedral Cu(II) complexes with CuN_6 chromophores, the Cu(II)/Cu(I) redox potential becomes more positive with an increase in the axial Cu–N bond length. Thus, the weaker $Cu–N6_{amine}$ bond in **1** would dissociate easily, followed by electron addition, rendering the Cu(II)/Cu(I) redox potential more positive. Also, the Cu(II)/Cu(I) redox potential of $[Cu(trien)(bpy)]^{2+}$ **1** with a longer $Cu–N6_{amine}$ axial bond (**1**, 2.723; **2**, 2.670 Å) or higher 'static' distortion (*cf.* above) is more positive than that of $[Cu(trien)(phen)]^{2+}$ **2**. In short, the stronger σ-coordination of bpy in the axial direction would facilitate a dissociation of the *trans* axial $Cu–N_{amine}$ bond. We have shown earlier that the tetragonality of $[Cu(phen)_3](ClO_4)_2$ is lower (*T*, 0.875) than that (*T*, 0.952) of $[Cu(5,6\text{-dmp})_3](ClO_4)_2$, illustrating the more positive Cu(II)/Cu(I) redox potential of the former complex (phen, 0.021; 5,6-dmp, −0.031 V).[18] Thus, the tetragonality of the octahedral Cu(II) complexes would determine the spectral, redox and other related properties.

DNA binding studies

UV-Vis absorption spectral titrations. One of the best experimental methods to investigate the mode and extent of interaction of metal complexes with DNA is electronic absorption spectral titration.[10] Upon stepwise addition of CT DNA to **1–4**,

Table 4 Absorption spectral titration of Cu(II) complexes, [Cu(trien)(diimine)]$(ClO_4)_2$ **1–4** with CT DNA

Complex	λ_{max} (nm)	Change in absorbance	K_b ($\times 10^5$ M^{-1})
1	235	Hypochromism (3.4%)	0.030 ± 0.002
2	227	Hypochromism (2.8%)	0.66 ± 0.01
3	231	Hypochromism (4.8%)	1.63 ± 0.10
4	237	Hypochromism (4.7%)	2.27± 0.20

Measurements were made at R = 0–25, where R = [DNA]/[complex], concentrations of solutions of copper(II) complexes = 3.75×10^{-5} M (**1**) and 1.5×10^{-5} M (**2–4**).

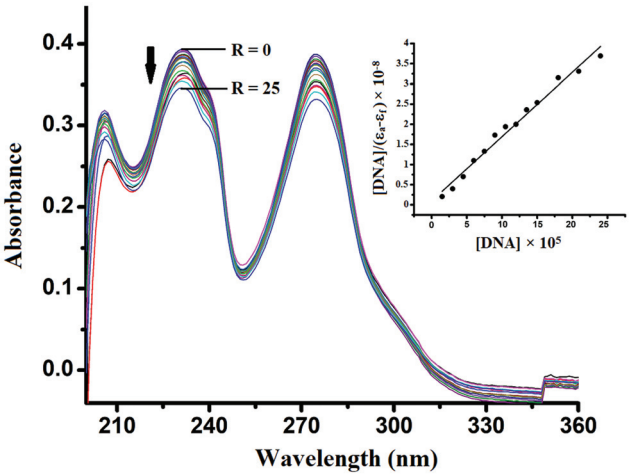

Fig. 3 Absorption spectra of [Cu(trien)(5,6-dmp)]$(ClO_4)_2$ **3** in 5 mM Tris-HCl buffer at pH 7.2, in the absence (R = 0) and presence (R = 1–25) of increasing amounts of CT DNA. Inset: the plot of [DNA] *vs.* [DNA]/($\varepsilon_a - \varepsilon_f$) at R = 25 of the complex [Cu(trien)(5,6-dmp)]$(ClO_4)_2$ **3**.

the ligand centered $\pi \rightarrow \pi^*$ absorption band (270–300 nm) shows hypochromism (3–5%, Table 4). The very small hypochromism, which is due to the slight partial filling of the empty π^* orbital of the co-ligand with the π electrons of the DNA base pair or distortions in DNA upon binding of the complex, and the absence of any red-shift reveals that the complexes do not partially intercalate into DNA base pairs. The DNA binding affinities of the complexes were estimated by calculating the DNA binding constant K_b by using the following equation,[52a,56,57]

$$[DNA]/(\varepsilon_a - \varepsilon_f) = [DNA]/(\varepsilon_b - \varepsilon_f) + 1/K_b(\varepsilon_b - \varepsilon_f)$$

where [DNA] is the concentration of DNA in base pairs, ε_a is the apparent extinction coefficient (= A_{obs}/[complex]), ε_f is the extinction coefficient of the complex in its free form and ε_b is the extinction coefficient of the complex in bound form. A straight line is observed when each set of data is plotted. The slope and y-intercept of the straight line are $1/(\varepsilon_b - \varepsilon_f)$ and $1/K_b(\varepsilon_b - \varepsilon_f)$ respectively,[10] and the ratio of the slope to intercept gives the value of K_b. The K_b value obtained for the complexes follows the order, K_b: **1** (0.030 ± 0.002) < **2** (0.66 ± 0.01) < **3** (1.63 ± 0.10) < **4** (2.27 ± 0.20 × 10^5 M^{-1}) (Table 4, Fig. 3 and S11–S13†), which reveals that the diimine co-ligand determines the DNA binding affinity, and that the diimine 'face' of the complex is involved in DNA binding (*cf.* below). The K_b value obtained for the phen complex **2** is thirty times higher than that observed ($2.1 \pm 0.2 \times 10^3$ M^{-1}) for the analogous five-coordinate complex [Cu(dien)(2,9-dmp)]$^{2+}$ (2,9-dmp = 2,9-dimethyl-1,10-phenanthroline), which has a structure similar to that of [Cu(dien)(phen)]$^{2+}$ (*cf.* above), but with a higher steric congestion at Cu(II).[23] The K_b value obtained for the 5,6-dmp complex **3** is again thirty times higher than that observed for the corresponding five-coordinate 3N ligand complex [Cu(dipica)(5,6-dmp)]$^{2+}$ ($4.4 \pm 0.2 \times 10^3$ M^{-1}).[23] All these observations suggest that the coordinatively saturated but axially elongated octahedral complexes **1–4**, rather than the corresponding coordinatively unsaturated square-based pyramidal complexes of the 3N ligands dien/dipica/bba/pmdt, would fit well with the DNA groove resulting in their stronger DNA binding. The hydrogen bonding propensity of the coordinated $-NH_2$ and –NH– groups of trien with the nucleobases or phosphate groups present in the edge of DNA, and the hydrophobic DNA interaction of the $-CH_2-CH_2-$ moieties, would also contribute to enhance the DNA binding affinity. A similar enhanced DNA binding affinity has been observed by us earlier for the octahedral complexes [Cu(tdp)(diimine)]$^{+}$ [58] and [$Ru(NH_3)_4$(diimine)]$^{2+}$.[59] Also, when the $-NH_2$ groups in [Cu(dien)(2,9-dmp)]$^{2+}$ are replaced with the pyridyl moieties to give [Cu(dipica)(2,9-dmp)]$^{2+}$, the DNA binding affinity decreases.[23] We have observed that the octahedral complex [Cu(5,6-dmp)$_3$]$^{2+}$ with a 'fluxional' coordination geometry (T, 0.952) binds with DNA (K_b, 3.8×10^4 M^{-1}) more strongly than [Cu(phen)$_3$]$^{2+}$ (K_b, 9.6×10^3 M^{-1}) with a 'static' coordination geometry (T, 0.875).[18] The DNA binding affinity of **2** is higher than that of **1**, which is expected due to the higher stereochemical 'fluxionality' in the absence of the partial intercalation of the planar phen ring (*cf.* above). The introduction of electron-releasing methyl groups[18] on the 5,6 (**3**) and 3,4,7,8 positions (**4**) on the phen ring is expected to confer a 'fluxional' stereochemistry higher than their phen analogue **2** (*cf.* above), and hence cause a significant increase in the DNA binding affinity. Also, complex **4** with four methyl groups on the phen ring would engage in a stronger hydrophobic interaction with the hydrophobic interior accessible in DNA, thus enhancing the DNA binding affinity higher than that of **3** with two methyl groups. Similar observations have been made by us earlier for the analogous complexes[20–25] of the type [Cu(L)(diimine)]$^{2+}$, where L is pmdt, dipica, bba, imda, *etc.*, bound to the CT DNA. Thus, the modification of the aromatic ring and number of methyl substituents on the co-ligands dictate the DNA binding structure and affinities of the present mixed-ligand complexes, and the hydrogen bonding propensity of the primary ligand increases the DNA binding affinity. It has been already established that copper(II) complexes, which possess higher DNA binding affinity, would display higher cytotoxicity.[4,44,52a] Thus, the 5,6-dmp (**3**) and 3,4,7,8-tmp (**4**) complexes with a higher DNA binding affinity would be expected to show cytotoxicity

higher than the corresponding bpy (**1**) and phen (**2**) complexes. However, interestingly, the bpy complex shows cytotoxicity higher than the other complexes (*cf.* below).

DNA docking studies

To validate and understand the mode and nature of DNA binding, a docking study of the complexes with 1BNA was employed (Fig. S14†). All complexes, irrespective of the co-ligands, prefer to dock on the DNA minor groove, which is in accordance with the above experimental observations. When the complexes bind to the polyanionic DNA, no change in the DNA turn length (36.3 Å) is observed, revealing that the structures of the complexes and the host DNA do not undergo any change upon binding. All complexes with an elongated octahedral shape bind to DNA with their diimine co-ligands preferably facing the DNA minor groove and the four nitrogen atoms of trien protruding out of the groove, and no evidence for the partial intercalation of the phen co-ligand of **2** is found. Also, the Patchdock atomic contact energies (ACE) obtained for the 'receptor-complex' docked structures (**1**, −330.38; **2**, −301.47; **3**, −385.48; **4**, −340.00 kcal mole^{-1}) reveal that the binding energies calculated fail to correlate well with the experimentally determined values of the DNA binding affinity (K_b). This illustrates that the hydrophobicity of 5,6-dmp in **3** contributes significantly to DNA binding interaction.

DNA cleavage studies

The DNA damage induced by certain anticancer agents has been approved as the cause of cell death,[60] and the *in vitro* cytotoxicity of many copper(II) complexes has been correlated with their DNA cleavage ability.[17,60–63] We have now studied the ability of **1–4** to cleave DNA by incubating them with a supercoiled (SC) pUC19 DNA (40 μM) in the absence of an external agent in 5 mM Tris-HCl/50 mM NaCl buffer at pH 7.2 for 1 h at 37 °C (Table S3 and Fig. S15†). All complexes convert the supercoiled (SC) form of DNA into a nicked circular (NC) form, while the control experiment with DNA does not show any apparent cleavage. Among the present complexes, **4** effects better DNA cleavage, which is in line with its stronger DNA interaction (*cf.* below) causing higher distortions on DNA. Also, when its concentration is varied from 50 to 500 μM, more than 50% of DNA cleavage is observed but only at a higher concentration (500 μM) (Table S4 and Fig. S16†). The DNA cleavage ability (15–29%) even at a 200 μM concentration is lower than the analogous [Cu(3N)(diimine)]$^{2+}$ complexes,[24,25] where 3N is pmdt, and bba. It is evident that the primary ligand trien tends to stabilize Cu(II) more than the Cu(I) form required to effect DNA cleavage.[64a] The absence of any partial intercalation to stabilize intimate contact of the Cu(I) form of complexes with DNA would also contribute significantly to the lower DNA cleavage observed.

The ability of **1–4** (100 μM) to cleave DNA oxidatively has also been investigated in the presence of ascorbic acid (10 μM) (Table 5 and Fig. 4). No apparent DNA cleavage is observed in the control experiments with DNA and the reducing agent. However, all complexes, except **1**, convert the SC form of DNA to the NC form to an extent of more than 50%, which is in contrast to the hydrolytic DNA cleavage ability observed. The lower ability of **1** to effect oxidative DNA cleavage, in spite of its higher ability to stabilize the Cu(I) oxidation state (*cf.* above) and hence Cu(I)-oxo species responsible for the oxidative DNA cleavage,[18,58] may be attributed to the inability of the bpy co-ligand with no extended aromatic ring to locate its Cu(I) form close to the place of cleavage reaction and to its weak surface binding with DNA.[24] Also, the higher DNA cleavage ability of **3** and **4** can be associated with the π-accepting property of the co-ligands stabilizing the Cu(I)-oxo species responsible for the oxidative DNA cleavage.[18,64a] The analogous dien complexes [Cu(dien)(bpy)]$^{2+}$ and [Cu(dien)(phen)]$^{2+}$ (30–50 μM) show a double strand DNA cleavage but only in the presence of a higher concentration (600 μM) of ascorbic acid, revealing that they have lower DNA cleavage potentials.

Table 5 Oxidative cleavage data of SC pUC19 DNA (40 μM) by complexes **1–4** (100 μM) in the presence of H_2A (10 μM) for an incubation time of 1 h

		Form (%)	
Lane number	Reaction conditions	SC	NC
1	DNA	97.2	2.8
2	DNA + H_2A (10 μM)	93.5	6.5
3	DNA + H_2A (10 μM) + **1** (100 μM)	74.3	25.7
4	DNA + H_2A (10 μM) + **2** (100 μM)	45.9	54.1
5	DNA + H_2A (10 μM) + **3** (100 μM)	5.4	94.6
6	DNA + H_2A (10 μM) + **4** (100 μM)	1.0	99.0

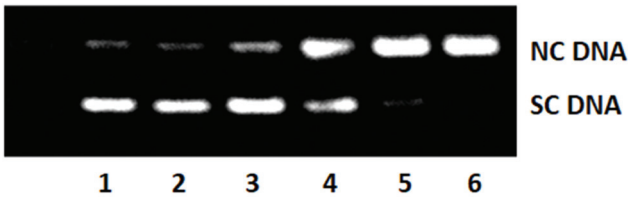

Fig. 4 Oxidative cleavage of supercoiled pUC19 DNA (40 μM) in the presence of ascorbic acid (H_2A, 10 μM) by copper(II) complexes **1–4** (100 μM) in a buffer containing 5 mM Tris HCl/50 mM NaCl at 37 °C; Lane 1, DNA; Lane 2, DNA + H_2A; Lane 3, DNA + **1** + H_2A; Lane 4, DNA + **2** + H_2A; Lane 5, DNA + **3** + H_2A; Lane 6, DNA + **4** + H_2A. SC and NC are supercoiled and nicked circular forms of DNA respectively.

Antiproliferative studies

Cytotoxicity studies. The ability to bind and damage DNA is considered to be one of the prerequisites for a drug to show potent cytotoxicity. As complexes **1–4** show both hydrolytic and oxidative DNA cleavage, we investigated their cytotoxicity along with their dien analogues [Cu(dien)(diimine)]$^{2+}$, Cu^{2+} ($Cu(ClO_4)_2{\cdot}6H_2O$), trien and diimine co-ligands, in comparison with the widely used anticancer drug doxorubicin under identical conditions (1 μg mL^{-1} used for all the cells) by using the MTT assay. For the present study, MCF-7 human breast and A549 human lung carcinoma cell lines were chosen. They were

Table 6 IC_{50} values of trien and diimine ligands, $Cu(ClO_4)_2{\cdot}6H_2O$ and dien and trien (**1–4**) complexes against MCF-7 and A549 cancer cell lines

Compounds	MCF-7 (μM)	A549 (μM)
Trien	7.6 ± 0.6	12.8 ± 0.4
$Cu(ClO_4)_2{\cdot}6H_2O$	6.4 ± 0.3	16.3 ± 0.6
$[Cu(dien)(bpy)]^{2+}$	12.7 ± 0.3	16.7 ± 0.6
$[Cu(dien)(phen)]^{2+}$	4.2 ± 0.5	4.1 ± 0.2
bpy	4.7 ± 0.5	5.3 ± 0.3
Phen	6.1 ± 0.5	7.1 ± 0.5
5,6-dmp	5.9 ± 0.9	5.9 ± 0.6
3,4,7,8-tmp	6.4 ± 0.2	4.6 ± 0.9
$[Cu(trien)(bpy)](ClO_4)_2$ **1**	3.9 ± 0.6	3.3 ± 0.2
$[Cu(trien)(phen)](ClO_4)_2$ **2**	11.3 ± 0.2	10.5 ± 0.2
$[Cu(trien)(5,6\text{-dmp})](ClO_4)_2$ **3**	2.1 ± 0.9	25.6 ± 0.3
$[Cu(trien)(3,4,7,8\text{-tmp})](ClO_4)_2$ **4**	>50	18.8 ± 0.2

treated with increasing concentrations of complexes and incubated for 48 h. An analysis of the IC_{50} values determined (Tables 6 and S5†) reveals that all complexes show significant cytotoxicity depending upon the cell lines. Thus, the potential of the complexes to kill cancer cells is found to vary as **1** > **2** > **4** > **3** for the A549 lung cancer cells, but as **3** > **1** > **2** > **4** for the MCF-7 cancer cells. It is surprising that **3** is very active against the MCF-7 cell lines, but least active towards the A549 cells, and **4** is reasonably active towards the A549 cells but extremely inactive towards the MCF-7 cells. This is expected because in the cellular system the same complex may not react similarly or may not follow the same mechanism as the characteristic of each cell line differs from one another. Thus, MCF-7 is a caspase 3 deficient cell, whereas A549 has a functional caspase 3. Again, the A549 cell is hormone independent, whereas the MCF-7 cell is hormone dependent; and the MCF-7 cell is estrogen positive but progesterone and HER negative. Likewise, there may be many other reasons for the observed differential effects of the complexes in different cell lines, and the effects may even vary in *in vitro* and *in vivo* conditions.[64b,c]

The free ligands, trien, bpy, phen, 5,6-dmp and 3,4,7,8-tmp, as well as aqueous Cu^{2+}, show moderate to good cytotoxicity (IC_{50}, 4.1–16.7 μM) against the MCF-7 and A549 cell lines. Interestingly, the bpy complex **1** shows a higher cytotoxicity (IC_{50}: MCF-7, 3.9(± 0.6); A549, 3.3(± 0.2) μM) than the aqueous Cu^{2+} ion, and bpy and trien ligands, revealing that complexation enhances the cytotoxicity of **1**. It exhibits a higher cytotoxicity than its five-coordinate $[Cu(dien)(bpy)]^{2+}$ analogue towards both MCF-7 (IC_{50}, 12.7(± 0.3)) and A549 (IC_{50}, 16.7(± 0.6) μM) cell lines. It appears that the octahedral complex **1**, because of its lower stereochemical fluxionality and higher compactness, would pass through the hydrophobic lipid bilayer of the cell membrane more easily than the square pyramidal dien complex into the cell to bind with cellular DNA more strongly and cause its damage. Also, it is more potent than its phen analogue **2** towards both MCF-7 (IC_{50}, 11.3(±0.2) μM) and A549 (IC_{50}, 10.5(±0.2) μM) cell lines, in spite of its DNA binding affinity being 30 times lower and DNA cleavage ability also lower (*cf.* above). The Cu(I) form of **1**, critically needed for DNA cleavage, is more easily formed upon reduction by the intracellular GSH than that of **2** (*cf.* above) so that it brings about a higher intracellular ROS generation (*cf.* below) and DNA damage, and hence the lower concentration of **1** is observed for killing 50% of cancer cells. Also, complex **2** with higher stereochemical fluxionality may tend to dissociate to give a five-coordinate complex species, and the hydrophilicity of the uncoordinated amine group[9a] would retard its transport across the bio-membrane. Interestingly, it exhibits a lower cytotoxicity than its constituents, namely, the phen and trien ligands and also its dien analogue (IC_{50}: MCF-7, 4.2(±0.5); A549, 4.1(±0.2) μM), in spite of its higher ability to bind and cleave DNA, supporting the important role of the higher stereochemical fluxionality of the phen complex. All these observations are in contrast to the mixed ligand copper(II)-bpy complexes like $[Cu(nal)(bpy)(H_2O)]^+$ (IC_{50}, 7.5 μM in the MCF-7 cancer cells at 48 h)[10] and $[Cu(tdp)(bpy)]^+$ (0.91 μM; $[Cu(tdp)(3,4,7,8\text{-tmp})]^+$ (0.29 μM in the MCF-7 cancer cells at 48 h)[58] *etc.*, which show a much lower cytotoxicity than their phen analogues. Also, very recently, the complex $[Cu(L)_2(bpy)]$, where L = 2-thiophenecarboxylate, has been found to show a higher IC_{50} value of 63.5 μM for A549 cancer cells,[65a] and the bpy complexes such as $[Cu_2(2,2'\text{-bpy})_2(L^1)_4]$ and $[Cu(2,2'\text{-bpy})(L^2)_2]_n$, where HL^1 is 5-phenyltetrazole and HL^2 is 1*H*-tetrazole, have shown higher IC_{50} values (10–30 μM) for MCF-7 cells.[65b]

The 5,6-dmp complex **3** shows a (IC_{50}, 2.1± 0.9 μM) significantly higher potency towards the MCF-7 cells, but a lower potency (IC_{50}, 25.6± 0.3 μM) towards the A549 cancer cells, than its parent phen analogue **2**. The higher cytotoxicity of **3** may originate from its stronger DNA binding affinity, which arises from its higher stereochemical fluxionality and the enhanced hydrophobicity of the 5,6-dmp co-ligand.[21,46] A similar correlation has been observed for the mixed-ligand complexes $[Cu(L\text{-tyr})(5,6\text{-dmp})]^+$,[21] $[Cu_2(LH)_2(5,6\text{-dmp})_2(ClO_4)_2]^{2+}$,[46] $[Cu(nal)(5,6\text{-dmp})(H_2O)](ClO_4)$, (H(nal) = nalidixic acid),[10] $[Cu(bba)(5,6\text{-dmp})](ClO_4)_2$ (bba = *N*,*N*′-bis(benzimidazol-2-ylmethyl)amine),[24] $[Cu(tdp)(5,6\text{-dmp})]^+$ (H(tdp) = 2-[(2-(2-hydroxyethylamino)ethylimino)methyl]phenol),[58] [Cu(L)(bpy)], (H_2L = *N*-(1-phenyl-3-methyl-4-(4-fluorobenzoyl)-5-pyrazolone)-2-salicylidenehydrazide)[65c] *etc.*, which exhibit a DNA binding affinity higher than their bpy and phen analogues.

However, under similar conditions, the biomembrane of the A549 cell line does not appear to facilitate (*cf.* above) the transport of **3** and **4**, both with the hydrophobic co-ligands. Complex **4**, unlike **3**, shows an extremely low cytotoxic potential towards MCF-7 (IC_{50}, >50 μM), but better potential towards the A549 (IC_{50}, 18.8 ± 0.2 μM) cell lines, which is unexpected given its stronger DNA binding affinity (*cf.* above). As observed for **2**, the higher stereochemical fluxionality of **4** conferred by the electron-releasing 3,4,7,8-tmp co-ligand would tend to form five-coordinate complex species, and the resulting uncoordinated hydrophilic amine group[9a] would retard the passage of the complex through the cell membrane.

As complexes **1** and **2** demonstrate the most potent cytotoxicity towards the MCF-7 and A549 cell lines, they were selected for further studies like ROS generation, mode of cell death *etc*. (*cf.* below).

Study of intracellular ROS generation. It is well known that redox-active metal complexes are capable of generating reactive oxygen species (ROS) in the cellular environment to cause cell death. We have shown earlier that redox-active [Cu(bba)(diimine)]ClO_4 complexes can induce ROS generation and hence apoptotic cell death (*cf.* below) *via* the oxidative stress pathway.[24,25] In order to identify the ROS responsible for the observed cytotoxicity of **1–4**, a study of intracellular ROS generation was undertaken. When 2′,7′-dichlorofluroescein diacetate (DCFH-DA) diffuses through the cell membrane, it is enzymatically hydrolyzed by intracellular esterases to form the non-fluorescent compound 2′,7′-dichlorofluroescein (DCFH). The latter is then rapidly oxidized to form the strongly fluorescent 2′,7′-dichlorofluroscein (DCF) in the presence of the ROS generated intracellularly. The ability of **1–4** to produce ROS in A549 lung cancer cells has been examined by using the fluorescent probe DCFH-DA. When the cancer cells are treated with an increasing concentration of complexes (0–50 μM) for 6 h, an increase in the intracellular ROS, as measured by the increase in the fluorescence intensity of DCF, is observed for all complexes in comparison with the control (Fig. 5). Also, the amount of intracellular ROS generated by the complexes follows the order **1** > **2** > **3** > **4**, which parallels the trend in the $E_{1/2}$ values of the complexes (*cf.* above). Indeed, at 50 μM concentration, **1** induces the generation of the intracellular ROS with an amount 7-fold higher than the untreated control, and **2**, **3** and **4** generate respectively 3.5, 2.1 and 2.0 fold higher intracellular ROS. Thus, the highest amount of ROS generated by **1** correlates with its highest ability to stabilize the Cu(I) oxidation state needed to produce the ROS in a cellular environment, illustrating the higher cytotoxicity of **1**. Also, the observation of a dose dependent increase in ROS generation confirms the involvement of Cu(II) to Cu(I) reduction for all four complexes under cellular conditions through the Fenton type reaction.

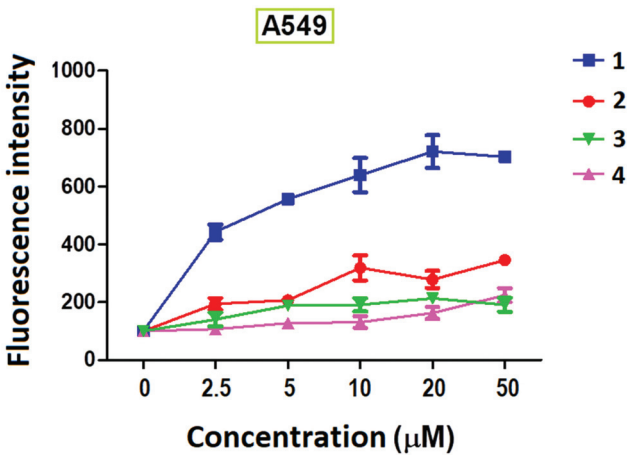

Fig. 5 Intracellular ROS generation in A549 cells. Fluorescence intensity after ROS generation in A549 cells after 6 h treatment. H_2O_2 (1 mM) was used as a positive control. Data represent the mean ± SD of three independent experiments.

Study of apoptosis using Annexin V.Cy3 staining assay. To evaluate the mode of cell death induced by **1** and **2** in the MCF-7 and A549 cell lines, further experiments were performed at two selected concentrations, one IC_{50} concentration and a concentration higher than the IC_{50} values of **1** and **2**. The translocation of phosphatidylserine from the cytoplasmic interface to the extracellular surface is one of the early features of apoptosis, and such a loss of membrane symmetry can be assessed by adopting Annexin V.Cy3 staining assay. To understand if induction of apoptosis is the primary basis of cytotoxicity, the cancer cells were treated with **1** and **2** for 24 h and subjected to apoptosis assay using fluorescent dyes (Fig. 6(A)). The cells were counted from multiple fields and categorized as live cells (only green fluorescent), apoptotic cells (both green and red fluorescent) and late apoptotic cells (only red fluorescent).[66] The percentages of cells undergoing early and late apoptosis after treatment with complexes **1** and **2** are indicated in Fig. 6(B). The quantification of the data reveals that **1**, at concentrations of 4 and 8 μM, induces apoptosis by 47% (early, 36; late, 11%) and 57% (early, 46; late, 11%) in A549 and 87 (early, 81; late, 6%) and 88% (early, 68; late, 20%) in the MCF-7 cells, respectively (Fig. 6(B)). The treatment of complex **2** at 10 and 20 μM concentrations induces apoptosis by 58 (early, 49, late, 9%) and 65% (early, 48, late, 17%) in the A549 cells and by 60 (early, 56, late, 4%) and 80% (early, 60, late, 20%) respectively in the MCF-7 cells (compared to the untreated controls). In the MCF-7 cells the untreated control cells show 2.2% early apoptotic and almost no late apoptotic cells. Thus both **1** and **2** show promising apoptosis-inducing efficacies, and **1** might be a superior drug, as a lower concentration of **1** is employed. The higher apoptosis-inducing ability of **1** is consistent with its more 'static' octahedral stereochemistry, which facilitates penetration into the cell membrane and the formation of Cu(I) species to generate a higher amount of ROS species involved in inducing apoptotic cell death. This is interesting because a number of five-coordinate complexes with the bpy co-ligand, which we have studied so far, have been found to show only a lower ability to induce apoptotic cell death than their corresponding phen, 5,6-dmp, and 3,4,7,8-tmp analogues.[24] Thus, both **1** and **2** induce cell death by apoptosis as the major mode of death.

DNA laddering assay: induction of apoptosis in the MCF-7 and A549 cancer cells. Apoptosis is the normal way of cell death in all types of cells and could be detected by using DNA laddering assay. When cells undergo apoptosis, the DNA in the cells starts degrading, and a ladder-like smear of fragmented DNA is seen in the agarose gel. When **1** and **2** at concentrations indicated in Fig. S17† were treated with MCF-7 and A549 cancer cells for 48 h, the inter-nucleosomal cleavage of DNA resulting in the formation of a "ladder" type DNA is visualized by using agarose gel electrophoresis. Although a sharp DNA ladder pattern is not obtained, a visible smear of fragmented DNA is observed in the MCF-7 and A549 cancer cells in comparison with the untreated control gel (Fig. S17†).[67] This supports the efficacy of bpy and phen complexes to induce apoptosis of cells in the early stages in both cells,

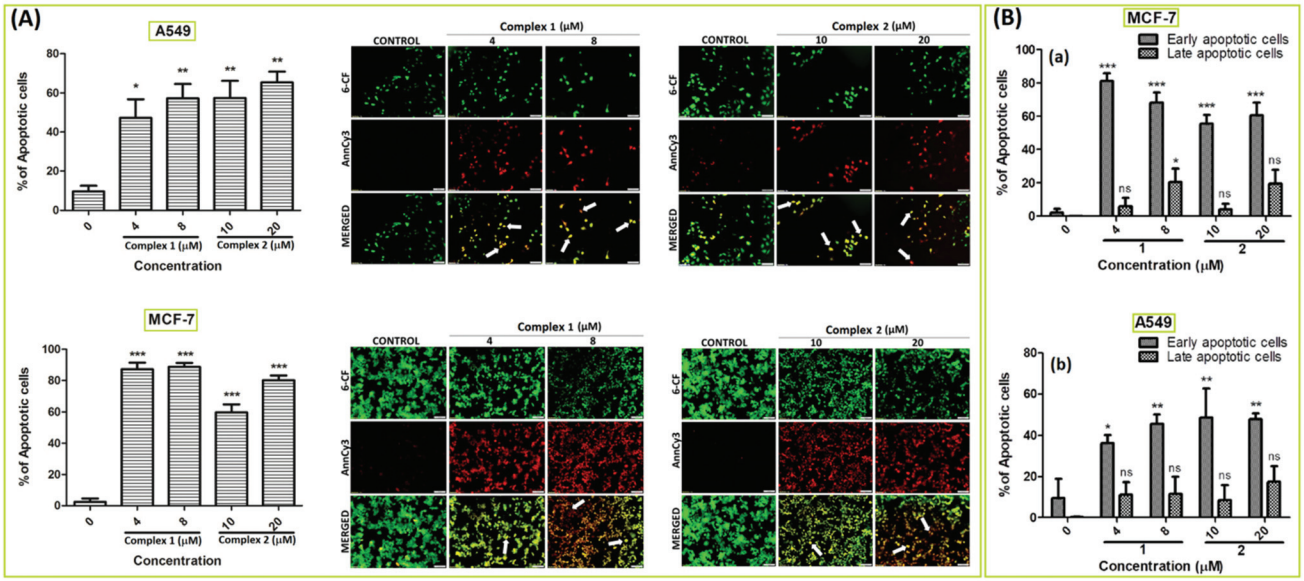

Fig. 6 (A) Fluorescence microscopic images showing features of Annexin V-Cy3.18 staining on A549 and MCF-7 cancer cells. Cells were treated with [Cu(trien)(bpy)]$(ClO_4)_2$ **1** (4, 8 μM) and [Cu(trien)(phen)]$(ClO_4)_2$ **2** (10, 20 μM) for 24 h. (Scale bar = 100 μm). (B) Percentage of apoptotic cells in early and late stages after 24 h treatment for complexes **1** and **2** in (a) MCF-7 and (b) A549 cells is represented. Data represent the mean ± SD of three independent experiments (ns = nonsignificant).

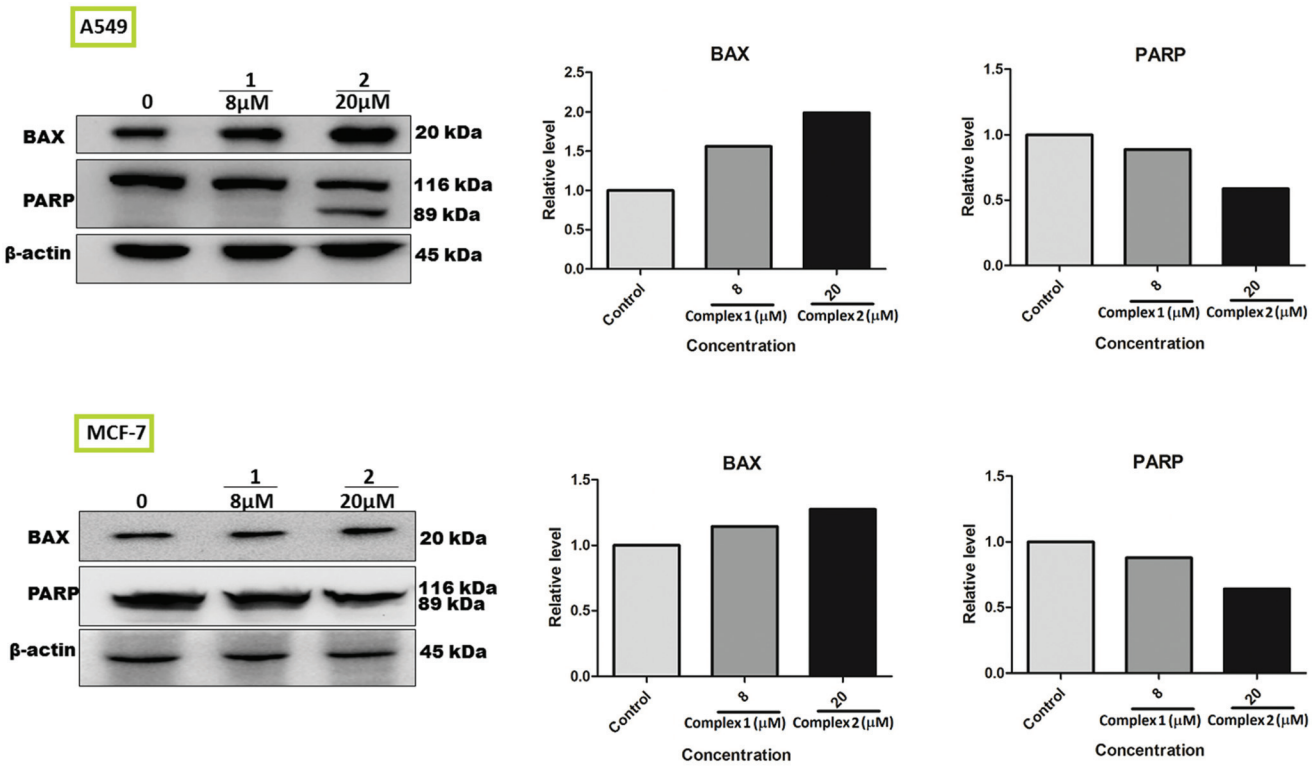

Fig. 7 Western blot analysis to study the expression of BAX and PARP in A549 and MCF-7 cancer cells following treatment with complexes [Cu(trien)(bpy)]$(ClO_4)_2$ **1** (8 μM) and [Cu(trien)(phen)]$(ClO_4)_2$ **2** (20 μM) for 24 h. The relative expression of the proteins after normalization with β-actin is shown in the right panels.

suggesting that the complexes are potential drugs for treating these cancers.

Effect of complexes on apoptosis-inducing proteins: western blot analysis. To confirm the apoptosis-inducing ability of **1** and **2**, the expression of apoptosis-associated proteins like Bax and PARP (Poly ADP-ribose polymerase) was analyzed for cancer cells treated with **1** and **2** (Fig. 7). Bax is an indicator of cellular apoptosis which increases the permeability of mitochondrial membrane leading to the release of cytochrome *c* from mitochondria and initiation of the caspase activation pathway for apoptosis.[68,69] Both complexes **1** and **2** are found to augment the expression of the pro-apoptotic Bax in comparison with untreated control. PARP helps cells to maintain their viability, and the cleaved or reduced amount of PARP serves as a marker of cells undergoing apoptosis as they facilitate cellular disassembly. When PARP is subsequently used by caspases as a substrate leading to increased caspase activity in the cells, a decrease in the concentration of PARP occurs.[70,71] Upon treatment of complexes **1** and **2** with cancer cells, either cleavage or reduction in PARP expression is observed. The cleavage of PARP is significant in A549 cells treated with 20 μM concentration of **2**; nevertheless, all other treatments show a reduction of PARP expression. So, it is clear that the bpy (**1**) and phen (**2**) complexes show promising cytotoxic and apoptosis-inducing activity and so they are proposed as possible therapeutic agents for cancer therapy. Further mechanistic and cellular uptake studies are essential to establish the higher potency of the complexes to kill cancer cells. We had successfully used western blot analysis of p53, Bax and Bcl-2 in MCF-7 and MDA-MB-231 cell lines for the mononuclear Cu(II) complex $[Cu(L)(diimine)]^+$, where LH = 2-[(2-dimethyl-aminoethylimino)methyl]phenol and diimine = dipyrido[3,2-*a*:2′,3′-c]phenazine (dppz).[72] The pro-apoptotic Bax is found to be up-regulated, and the antiapoptotic Bcl-2 is down-regulated in the treated cells, which reveal that the cells undergo apoptosis through the intrinsic mitochondrial pathway. We had also shown that the treatment with the Cu(II) complex results in a decrease in the levels of pro-caspases and concomitant increase in the levels of cleaved caspase, which is confirmed by the increase in the levels of cleaved PARP.[72–74]

Conclusions

Four mixed ligand complexes of the type $[Cu(trien)(diimine)](ClO_4)_2$ have been synthesized and their DNA binding and cleavage ability and cytotoxicity studied. In the single-crystal X-ray structures, the bpy and phen complexes possess an axially elongated octahedral coordination geometry around Cu(II). All complexes, depending upon the diimine co-ligand, display varying stereochemical fluxionality which illustrates the trends in their ligand field energy, Cu(II)/Cu(I) redox potential and DNA binding affinity. Thus, the bpy complex with a more 'static' stereochemistry and hence higher Cu(II)/Cu(I) redox potential induces the generation of a maximum amount of intracellular ROS, which accounts for its higher cytotoxicity towards MCF-7 human breast carcinoma (IC_{50}, 3.9 μM) and A549 human lung carcinoma (IC_{50}, 3.3 μM) cell lines compared to its phen analogue. Also, the Cu(II) complex of the 5,6-dmp co-ligand, with stereochemical 'fluxionality' higher than its phen analogue, shows a lower Cu(II)/Cu(I) redox potential, higher DNA binding affinity and higher cytotoxicity (IC_{50}, 2.1 μM) towards the MCF-7 cell line. The 3,4,7,8-tmp complex shows an extremely low cytotoxic potential towards MCF-7 (IC_{50}, >50 μM) but better cytotoxicity towards the A549 (IC_{50}, 18.8 μM) cell lines. The poor cytotoxicity of the complex is unexpected due to its stronger DNA binding involving the hydrophobic 3,4,7,8-tmp co-ligand, and it is in line with its lowest Cu(II)/Cu(I) redox potential, and hence the lowest amount of ROS is generated. All complexes, irrespective of the type of the diimine co-ligand, prefer to dock on the DNA minor groove with their trien ligand protruding out of the groove. The bpy and phen complexes display the potential to kill cancer cell lines, preferably in the apoptotic mode, as revealed by the Annexin V.Cy3 staining assay. Western blot analysis confirms this observation and throws light on the onset of caspase activity when cancer cells are treated with the complexes. Further mechanistic and cellular uptake studies are essential to confirm the higher potency of the octahedral Cu(II)-diimine complexes of trien to induce apoptotic killing in cancer cells, and hence to develop them as promising drugs for cancer therapy.

Conflicts of interest

There are no conflicts to declare.

Acknowledgements

We thank INSA, New Delhi, for the INSA Senior Scientist position and the Science and Engineering Research Board (SERB), New Delhi, for a research project with financial support (EMR/2015/002222) to M. P. We are thankful to Dr M. Velusamy, Department of Chemistry, North Eastern Hill University, Shillong, for help in solving the X-ray crystal structures and Miss A. Sanjeev, Department of Molecular Biology and Biotechnology, Tezpur University, Tezpur, for helping us with docking studies.

References

1 F. Bray, J. Ferlay, I. Soerjomataram, R. L. Siegel, L. A. Torre and A. Jemal, *Ca-Cancer J. Clin.*, 2018, **68**, 394–424.
2 A. V. Klein and T. W. Hambley, *Chem. Rev.*, 2009, **109**, 4911–4920.
3 (*a*) A. Atmaca, S. Al-Batran, D. Werner, C. Pauligk, T. Güner, A. Koepke, H. Bernhard, T. Wenzel, A. Banat and P. Brueck, *Br. J. Cancer*, 2013, **108**, 265; (*b*) M. Ganeshpandian, M. Palaniandavar, A. Muruganantham, S. K. Ghosh, A. Riyasdeen and M. A. Akbarsha, *Appl. Organomet. Chem.*,

2018, **32**, e4154; (*c*) T. Khamrang, R. Kartikeyan, M. Velusamy, V. Rajendiran, R. Dhivya, B. Perumalsamy, M. A. Akbarsha and M. Palaniandavar, *RSC Adv.*, 2016, **6**, 114143–114158; (*d*) C. R. Munteanu and K. Suntharalingam, *Dalton Trans.*, 2015, **44**, 13796–13808; (*e*) T. Bal-Demirci, G. Congur, A. Erdem, S. Erdem-Kuruca, N. Özdemir, K. Akgün-Dar, B. Varol and B. Ülküseven, *New J. Chem.*, 2015, **39**, 5643–5653; (*f*) U. M. Rafi, D. Mahendiran, A. K. Haleel, R. P. Nankar, M. Doble and A. K. Rahiman, *New J. Chem.*, 2016, **40**, 2451–2465.

4 R. Loganathan, S. Ramakrishnan, M. Ganeshpandian, N. S. Bhuvanesh, M. Palaniandavar, A. Riyasdeen and M. A. Akbarsha, *Dalton Trans.*, 2015, **44**, 10210–10227.

5 S. Lippard and J. Berg, *Principles of bioinorganic chemistry*, University Science Books, Mill Valley, California, 2005, vol. xvii.

6 (*a*) M. Palaniandavar, S. Indira, M. Lakshminarayanan and H. Manohar, *J. Chem. Soc., Dalton Trans.*, 1996, **7**, 1333–1340; (*b*) M. Chikira, C. Ng and M. Palaniandavar, *Int. J. Mol. Sci.*, 2015, **16**, 22754–22780.

7 C. Santini, M. Pellei, V. Gandin, M. Porchia, F. Tisato and C. Marzano, *Chem. Rev.*, 2013, **114**, 815–862.

8 C. Marzano, M. Pellei, F. Tisato and C. Santini, *Anti-Cancer Agents Med. Chem.*, 2009, **9**, 185–211.

9 (*a*) R. Patel, N. Singh, K. Shukla, J. Niclós-Gutiérrez, A. Castineiras, V. Vaidyanathan and B. U. Nair, *Spectrochim. Acta, Part A*, 2005, **62**, 261–268; (*b*) I. Turel, *Coord. Chem. Rev.*, 2002, **232**, 27–47.

10 R. Loganathan, M. Ganeshpandian, N. S. Bhuvanesh, M. Palaniandavar, A. Muruganantham, S. K. Ghosh, A. Riyasdeen and M. A. Akbarsha, *J. Inorg. Biochem.*, 2017, **174**, 1–13.

11 M. E. Katsarou, E. K. Efthimiadou, G. Psomas, A. Karaliota and D. Vourloumis, *J. Med. Chem.*, 2008, **51**, 470–478.

12 E. K. Efthimiadou, M. E. Katsarou, A. Karaliota and G. Psomas, *J. Inorg. Biochem.*, 2008, **102**, 910–920.

13 A. R. Chakravarty, *J. Chem. Sci.*, 2006, **118**, 443–453.

14 D. Sigman, D. Graham, V. D'aurora and A. Stern, *J. Biol. Chem.*, 1979, **254**, 12269–12272.

15 A. Spassky and D. S. Sigman, *Biochemistry*, 1985, **24**, 8050–8056.

16 J. D. Ranford, P. J. Sadler and D. A. Tocher, *Dalton Trans.*, 1993, 3393–3399.

17 H. E. L. Hegg and J. N. Burstyn, *Coord. Chem. Rev.*, 1998, **173**, 133–165.

18 S. Ramakrishnan and M. Palaniandavar, *Dalton Trans.*, 2008, **29**, 3866–3878.

19 N. A. Mazlan, T. B. S. Ravoof, E. R. Tiekink, M. I. M. Tahir, A. Veerakumarasivam and K. A. Crouse, *Transition Met. Chem.*, 2014, **39**, 633–639.

20 B. Selvakumar, V. Rajendiran, P. U. Maheswari, H. Stoeckli-Evans and M. Palaniandavar, *J. Inorg. Biochem.*, 2006, **100**, 316–330.

21 S. Ramakrishnan, V. Rajendiran, M. Palaniandavar, V. S. Periasamy, B. S. Srinag, H. Krishnamurthy and M. A. Akbarsha, *Inorg. Chem.*, 2009, **48**, 1309–1322.

22 P. Jaividhya, R. Dhivya, M. A. Akbarsha and M. Palaniandavar, *J. Inorg. Biochem.*, 2012, **114**, 94–105.

23 S. Ramakrishnan and M. Palaniandavar, *J. Chem. Sci.*, 2005, **117**, 179–186.

24 R. Loganathan, S. Ramakrishnan, E. Suresh, A. Riyasdeen, M. A. Akbarsha and M. Palaniandavar, *Inorg. Chem.*, 2012, **51**, 5512–5532.

25 M. Ganeshpandian, R. Loganathan, S. Ramakrishnan, A. Riyasdeen, M. A. Akbarsha and M. Palaniandavar, *Polyhedron*, 2013, **52**, 924–938.

26 J. Lu, *Mol. Cancer Ther.*, 2010, **9**, 2458–2467.

27 (*a*) V. M. Nurchi, G. Crisponi, M. Crespo-Alonso, J. I. Lachowicz, Z. Szewczuk and G. J. Cooper, *Dalton Trans.*, 2013, **42**, 6161–6170; (*b*) G. J. Cooper, *Drugs*, 2011, **71**, 1281–1320; (*c*) R. S. Kumar, S. Arunachalam, V. S. Periasamy, C. P. Preethy, A. Riyasdeen and M. A. Akbarsha, *Aust. J. Chem.*, 2009, **62**, 165–175; (*d*) R. S. Kumar and S. Arunachalam, *Biophys. Chem.*, 2008, **136**, 136–144; (*e*) B. Liu, J. Chai, X. Hu, Y. Zhang, J. Nan and B. Yang, *Inorg. Chem. Commun.*, 2015, **52**, 27–30.

28 J. Marmur, *J. Mol. Biol.*, 1961, **3**, 208–218.

29 C. R. Merril, D. Goldman, S. A. Sedman and M. H. Ebert, *Science*, 1981, **211**, 1437–1438.

30 G. M. Sheldrick, *Acta Crystallogr., Sect. A: Found. Crystallogr.*, 2008, **64**, 112–122.

31 M. N. Burnett and C. K. Johnson, *Report ORNL-6895*, Oak Ridge National Laboratory, Tennessee, USA, 1996.

32 (*a*) M. Frisch, G. Trucks, H. Schlegel, G. Scuseria, M. Robb, J. Cheeseman, G. Scalmani, V. Barone, B. Mennucci and G. Petersson, *GAUSSIAN 09 (Revision D. 01)*, Gaussian. Inc., Wallingford, CT, 2009; (*b*) M. Atanasov, P. Comba, B. Martin, V. Müller, G. Rajaraman, H. Rohwer and S. Wunderlich, *J. Comput. Chem.*, 2006, **27**, 1263–1277.

33 (*a*) M. D. Hanwell, D. E. Curtis, D. C. Lonie, T. Vandermeersch, E. Zurek and G. R. Hutchison, *J. Cheminf.*, 2012, **4**, 17; (*b*) D. Duhovny, R. Nussinov and H. J. Wolfson, in *International workshop on algorithms in bioinformatics*, ed. R. Guigó and D. Gusfield, Springer, Berlin, Heidelberg, 2002, pp. 185–200.

34 C. Zhang, G. Vasmatzis, J. L. Cornette and C. DeLisi, *J. Mol. Biol.*, 1997, **267**, 707–726.

35 N. Andrusier, R. Nussinov and H. J. Wolfson, *Proteins*, 2007, **69**, 139–159.

36 C. L. Kingsford, B. Chazelle and M. Singh, *Bioinformatics*, 2004, **21**, 1028–1039.

37 T. Mosmann, *J. Immunol. Methods*, 1983, **65**, 55–63.

38 (*a*) M. V. Blagosklonny and W. S. El-Deiry, *Int. J. Cancer*, 1996, **67**, 386–392; (*b*) *Prism, GraphPad*, Graphpad software, San Diego, CA, USA, 1994.

39 A. Riyasdeen, V. S. Periasamy, P. Paul, A. A. Alshatwi and M. A. Akbarsha, *J. Evidence-Based Complementary Altern. Med.*, 2012, **2012**, 136527.

40 J. Foley, D. Kennefick, D. Phelan, S. Tyagi and B. Hathaway, *Dalton Trans.*, 1983, **10**, 2333–2338.

41 V. Rajendiran, M. Murali, E. Suresh, S. Sinha, K. Somasundaram and M. Palaniandavar, *Dalton Trans.*, 2008, 148–163.
42 R. N. Patel, M. K. Kesharwani, A. Singh, D. K. Patel and M. Choudhary, *Transition Met. Chem.*, 2008, **33**, 733–738.
43 J. E. Huheey, E. A. Keiter, R. L. Keiter and O. K. Medhi, *Inorganic chemistry: principles of structure and reactivity*, Pearson Education, India, 2006.
44 (*a*) M. Ganeshpandian, S. Ramakrishnan, M. Palaniandavar, E. Suresh, A. Riyasdeen and M. A. Akbarsha, *J. Inorg. Biochem.*, 2014, **140**, 202–212; (*b*) R. N. Patel, N. Singh, K. K. Shukla, J. Niclós-Gutiérrez, A. Castineiras, V. G. Vaidyanathan and B. U. Nair, *Spectrochim. Acta, Part A*, 2005, **62**, 261–268.
45 B. Murphy, M. Aljabri, A. M. Ahmed, G. Murphy, B. J. Hathaway, M. E. Light, T. Geilbrich and M. B. Hursthouse, *Dalton Trans.*, 2006, **2**, 357–367.
46 S. Ramakrishnan, D. Shakthipriya, E. Suresh, V. S. Periasamy, M. A. Akbarsha and M. Palaniandavar, *Inorg. Chem.*, 2011, **50**, 6458–6471.
47 B. J. Hathaway and P. G. Hodgson, *Polyhedron*, 1973, **35**, 4071–4081.
48 M. Ruiz, L. Perello, R. Ortiz, A. Castineiras, C. Maichle-Mössmer and E. Canton, *J. Inorg. Biochem.*, 1995, **59**, 801–810.
49 P. Nagle, E. O'Sullivan, B. J. Hathaway and E. Muller, *Dalton Trans.*, 1990, (11), 3399–3406.
50 P. T. Selvi, M. Murali, M. Palaniandavar, M. Köckerling and G. Henkel, *Inorg. Chim. Acta*, 2002, **340**, 139–146.
51 (*a*) M. Murali and M. Palaniandavar, *Dalton Trans.*, 2006, 730–743; (*b*) M. Murali and M. Palaniandavar, *Polyhedron*, 2007, **26**, 3980–3992.
52 (*a*) R. Loganathan, S. Ramakrishnan, E. Suresh, M. Palaniandavar, A. Riyasdeen and M. A. Akbarsha, *Dalton Trans.*, 2014, **43**, 6177–6194; (*b*) C. Krishnan, C. Creutz, H. A. Schwarz and N. Sutin, *J. Am. Chem. Soc.*, 1983, **105**, 5617–5623.
53 B. Hathaway and D. Billing, *Coord. Chem. Rev.*, 1970, **5**, 143–207.
54 M. Palaniandavar, I. Somasundaram, M. Lakshminarayanan and H. Manohar, *Dalton Trans.*, 1996, (7), 1333–1340.
55 (*a*) E. I. Solomon, K. W. Penfield and D. E. Wilcox, *Copper, Molybdenum, and Vanadium in Biological Systems*, Springer, 1983, pp. 1–57; (*b*) K. A. Rubinson, *J. Am. Chem. Soc.*, 1979, **101**, 6105–6110.
56 M. T. Carter, M. Rodriguez and A. J. Bard, *J. Am. Chem. Soc.*, 1989, **111**, 8901–8911.
57 M. Kumar, G. Kumar, N. K. Mogha, R. Jain, F. Hussain and D. T. Masram, *Spectrochim. Acta, Part A*, 2019, **212**, 94–104.
58 V. Rajendiran, R. Karthik, M. Palaniandavar, H. Stoeckli-Evans, V. S. Periasamy, M. A. Akbarsha, B. S. Srinag and H. Krishnamurthy, *Inorg. Chem.*, 2007, **46**, 8208–8221.
59 P. U. Maheswari and M. Palaniandavar, *Inorg. Chim. Acta*, 2004, **357**, 901–912.
60 S. Neidle and M. J. Waring, *Molecular aspects of anticancer drug-DNA interactions*, Macmillan International Higher Education, 1994.
61 R. Hudej, J. Kljun, W. Kandioller, U. K. Repnik, B. Turk, C. G. Hartinger, B. K. Keppler, D. Miklavčič and I. Turel, *Organometallics*, 2012, **31**, 5867–5874.
62 J. Kljun, I. Bratsos, E. Alessio, G. Psomas, U. k. Repnik, M. Butinar, B. Turk and I. Turel, *Inorg. Chem.*, 2013, **52**, 9039–9052.
63 Y. An, S.-D. Liu, S.-Y. Deng, L.-N. Ji and Z.-W. Mao, *J. Inorg. Biochem.*, 2006, **100**, 1586–1593.
64 (*a*) S. Mahadevan and M. Palaniandavar, *Inorg. Chem.*, 1998, **37**, 3927–3934; (*b*) M. C. Kowalczyk, Z. Walaszek, P. Kowalczyk, T. Kinjo, M. Hanausek and T. J. Slaga, *Carcinogenesis*, 2009, **30**, 1008–1015; (*c*) B. M. Schmidt, J. W. Erdman Jr. and M. A. Lila, *Cancer Lett.*, 2006, **231**, 240–246.
65 (*a*) Z. Boulsourani, G. Geromichalos, S. Katsamakas, V. Psycharis, C. Raptopoulou, D. Hadjipavlou-Litina, D. Sahpazidou and C. Dendrinou-Samara, *Mater. Sci. Eng., C*, 2019, **94**, 493–508; (*b*) J. A. Eremina, E. V. Lider, D. G. Samsonenko, L. A. Sheludyakova, A. S. Berezin, L. S. Klyushova, V. A. Ostrovskii and R. E. Trifonov, *Inorg. Chim. Acta*, 2019, **487**, 138–144; (*c*) J. Wang, G.-C. Xu, Y.-P. Zhang, H.-Y. Luo, J.-Y. Li, L. Zhang and D.-Z. Jia, *New J. Chem.*, 2019, **43**, 2529–2539.
66 E. Kimura, S. Aoki, E. Kikuta and T. Koike, *Proc. Natl. Acad. Sci. U. S. A.*, 2003, **100**, 3731–3736.
67 W. Gorczyca, J. Gong and Z. Darzynkiewicz, *Cancer Res.*, 1993, **53**, 1945–1951.
68 J. C. Reed, *J. Clin. Invest.*, 1996, **97**, 2403–2404.
69 Q. Zhan, S. Fan, I. Bae, C. Guillouf, D. A. Liebermann, P. M. O'Connor and J. A. Fornace, *Oncogene*, 1994, **9**, 3743–3751.
70 A. H. Boulares, A. G. Yakovlev, V. Ivanova, B. A. Stoica, G. Wang, S. Iyer and M. Smulson, *J. Biol. Chem.*, 1999, **274**, 22932–22940.
71 M. Germain, E. B. Affar, D. D'Amours, V. M. Dixit, G. S. Salvesen and G. G. Poirier, *J. Biol. Chem.*, 1999, **274**, 28379–28384.
72 R. Dhivya, P. Jaividhya, A. Riyasdeen, M. Palaniandavar, G. Mathan and M. A. Akbarsha, *BioMetals*, 2015, **28**, 929–943.
73 S. Haldar, M. Negrini, M. Monne, S. Sabbioni and C. M. Croce, *Cancer Res.*, 1994, **54**, 2095–2097.
74 C. M. Knudson and S. J. Korsmeyer, *Nat. Genet.*, 1997, **16**, 358.

